AD-A136 897 INVESTIGATION OF EFFECTS CONTRIBUTING TO DYNAMIC STALL USING A MOMENTUM-I..(U) AIR FORCE INST OF TECH WRIGHT-PATTERSON AFB OH SCHOOL OF ENGI.. J S LAWRENCE 1/2

UNCLASSIFIED DEC 83 AFIT/GAE/AA/83D-12 F/G 20/4 NL

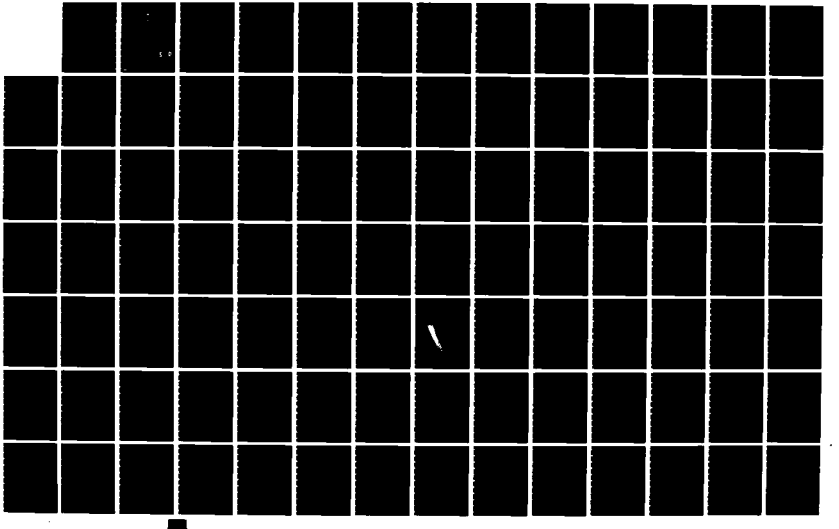

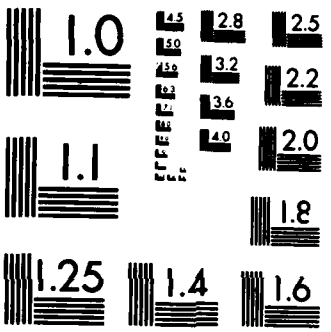

MICROCOPY RESOLUTION TEST CHART
NATIONAL BUREAU OF STANDARDS-1963-A

INVESTIGATION OF EFFECTS CONTRIBUTING TO DYNAMIC STALL USING A MOMENTUM-INTEGRAL METHOD

THESIS

AFIT/GAE/AA/83D-12

John S. Lawrence
Major USA

DEPARTMENT OF THE AIR FORCE
AIR UNIVERSITY
AIR FORCE INSTITUTE OF TECHNOLOGY

Wright-Patterson Air Force Base, Ohio

AFIT/GAE/AA/83D-12

INVESTIGATION OF EFFECTS CONTRIBUTING TO DYNAMIC STALL USING A MOMENTUM-INTEGRAL METHOD

THESIS

AFIT/GAE/AA/83D-12

John S. Lawrence
Major USA

AFIT/GAE/AA/83D-12

INVESTIGATION OF EFFECTS CONTRIBUTING TO DYNAMIC STALL USING A MOMENTUM-INTEGRAL METHOD

THESIS

Presented to the Faculty of the School of Engineering

of the Air Force Institute of Technology

Air University

in Partial Fulfillment of the

Requirements for the Degree of

Master of Science

by

John S. Lawrence, B.S.

Major USA

Graduate Aeronautical Engineering

December 1983

Acknowledgements

The scope of this investigation would have been greatly reduced if not for the ever constant aid and guidance of my thesis advisor, Major E. Jumper. His ability to give me the necessary technical insight into the problem while never losing sight of the basic physical principles involved was my key to success. Special thanks are also due to Dr. J. Hitchcock for his expert advice and assistance throughout the course of my work. Finally, I would like to thank my family for their enduring patience and support over the last year, sharing with me both my frustrations and elations.

John S. Lawrence

Table of Contents

List of Symbols

B	hypothetical body force
C	airfoil chord
C_l	coefficient of lift
K	boundary layer shape parameter
$\dot{m}$	mass flow rate
P	pressure
t	time
u	streamwise velocity in the boundary layer
U_e	streamwise velocity at the edge of the boundary layer
U_∞	free-stream velocity
v	velocity in the normal direction
x	distance variable in the flow direction
y	distance variable normal to the flow direction
α	angle of attack
$\dot{\alpha}$	pitch rate
δ	boundary layer thickness
δ_1	displacement thickness
δ_2	momentum thickness
Λ	boundary layer shape parameter
μ	viscosity
ν	kinematic viscosity
ρ	density
τ_w	wall shear
AR	aspect ratio

List of Figures

Abstract

Dynamic stall effects are analyzed in this investigation for cases of (1) an inertially static airfoil in a flow field rotating at constant rate (gust response), and (2) an airfoil pitching at constant rate in a steady flow field. The method used is a boundary layer solution of the momentum-integral equation by a modified von Karman-Pohlhausen technique.

Work accomplished by Docken in 1982 using this method to match Kramer's experimental results for gust response is reviewed, corrected, and continued. The validity of the closure equation and the assumptions key to its derivation are examined, concluding that the closure equation is justified. A better match of Kramer's airfoil sections results in dynamic stall predictions very close to experimental data. The effect of varying airfoil thickness and camber is investigated.

By consideration of the non-Newtonian motion of the boundary layer on the surface of a pitching airfoil, the momentum-integral method is extended to the second case. Using the Moore-Rott-Sears model for flow separation criteria, analytical results were computed and compared with experimental data. Reduction in adversity of the pressure gradient accounts for only a fraction of the total dynamic effect, and it is proposed that mass introduction into the boundary layer from the free-stream may be a strongly contributing factor. This phenomena is demonstrated to have a large effect, and an argument is presented for the proper amount of mass introduction.

INVESTIGATION OF EFFECTS CONTRIBUTING TO DYNAMIC STALL USING A MOMENTUM-INTEGRAL METHOD

I. Introduction

Discussion

Dynamic stall is a phenomenon that has received considerable attention over the past two decades. It is understandably of intense interest to the helicopter and compressor industries, where much of the research has been conducted, and more recently has received the attention of the aerospace industry in applications to winged space shuttle vehicles (Ref 23:2). The majority of the research has been experimental, and most of the analytical work has relied on some sort of experimental data as input. Further, because of the importance of practical application (i.e., helicopter blades), nearly all of the work in recent years has dealt with oscillatory motion of the airfoil. Consequently, there is still much to be learned and understood about the basic physical flow phenomena which contribute to dynamic stall.

The concept is not difficult. When an airfoil angle of attack is increased rapidly through a range that includes the static stall angle, the maximum lift and drag are significantly increased, stall is delayed to a higher angle of attack, and the corresponding loss of lift is often much more severe in nature. The problem then is one of complexity. Contributing factors are both viscous and inviscid. The phenomenon is strongly dependent

on the rate of pitch, free-stream velocity, and frequency and amplitude (for an oscillating airfoil), and shows varying degrees of dependence on airfoil shape, 3D flow effects, Reynolds number, and Mach number (Ref 1:304).

Problem Statement

It is far beyond the scope of this study to attempt to analytically predict dynamic stall effects on an airfoil. Rather, the purpose of this thesis is to attain a better physical understanding of some of the contributing causes of dynamic stall. As such, restriction is made to the analysis of boundary layer effects for an airfoil undergoing a constant rate of change in angle of attack. It would seem essential that the physics of this relatively simple problem should be well understood and documented prior to an analytical study of more complex oscillatory motions, but such has not been the case.

The method of analysis will be to integrate a solution of the unsteady (time-dependent) boundary layer equations, using a modified von Karman-Pohlhausen momentum-integral technique, until stall is indicated, and determine the maximum angle of attack at this point. Stall of the airfoil is here defined as the condition of flow separation at quarter-chord of the airfoil, with flow separation being initially defined as the condition of zero shear at the surface as indicated by the velocity profile shape parameter (this definition of separation is later modified using the MRS conditions for the case of a pitching wing). To use this technique, the classical boundary layer assumptions must be applied.

Two distinct cases will be analyzed. The first is that of an inertially

static airfoil in a rotating flow field, and this will heretofore be referred to as the "gust-response" problem. The second is that of a pitching airfoil in a steady flow field, and will be referred to as the "pitching airfoil" problem. These may appear at first to be the same problem, differing only in the reference frame of the observer. Experimental results, however, indicate greatly differing effects, as will be shown. The analysis of this report will also point out the differences between these two cases.

Background

Max Kramer reported the results of an experimental study of the gust-response problem in 1932. By fixing a wing section between a set of moveable guide vanes and a diffuser, he was able to take lift measurements while constantly varying the angle (with respect to chordline) of the free-stream velocity. Based on his results, Kramer established a linear relationship between the increase of maximum lift coefficient (over the steady flow case) and the non-dimensional pitch rate (Ref 2).

An analytic study of the gust-response problem conducted by Richard Docken in 1982 successfully predicted a relationship in close agreement with Kramer (Ref 3). He developed a modified von Karman-Pohlhausen integral method for unsteady flow and applied it to the boundary layer of a representative Joukowski airfoil. The outstanding feature of this method is the development of a closure equation to handle the unknown unsteady term.

Two experimental studies of the pitching airfoil problem are of particular interest. In 1978 Arthur Deekens and William Kuebler conducted smoke tunnel tests of an airfoil section pitching at various constant rates

and in various free-stream steady velocities. Motion pictures were taken of the flow, allowing observation of flow separation at quarter-chord versus instantaneous angle of attack. By comparison with static conditions, they were able to determine a direct correlation between the delay in stall angle of attack and the non-dimensional pitch rate (Ref 4). Daniel Daley found complimentary results to this in 1982 (Ref 5). He developed a microcomputer-based automatic data acquisition system such that flow separation on the surface of an airfoil section could be determined by pressure indications. Again, by varying pitch rates and steady free-stream velocities, data was taken, compared with static stall conditions, and results noted.

The results of the work by Daley, Deekens and Kuebler, and Kramer are shown in Figure 1. Note the difference in effect between the gust response problem and the pitching airfoil problem. Docken shows in his work that the dynamic effect in the gust-response problem is the result of a reduction in the adversity of the pressure gradient in unsteady flow. The extent of this effect on a pitching airfoil and what, if any, other phenomena are contributing to dynamic stall, are matters to be investigated in this study.

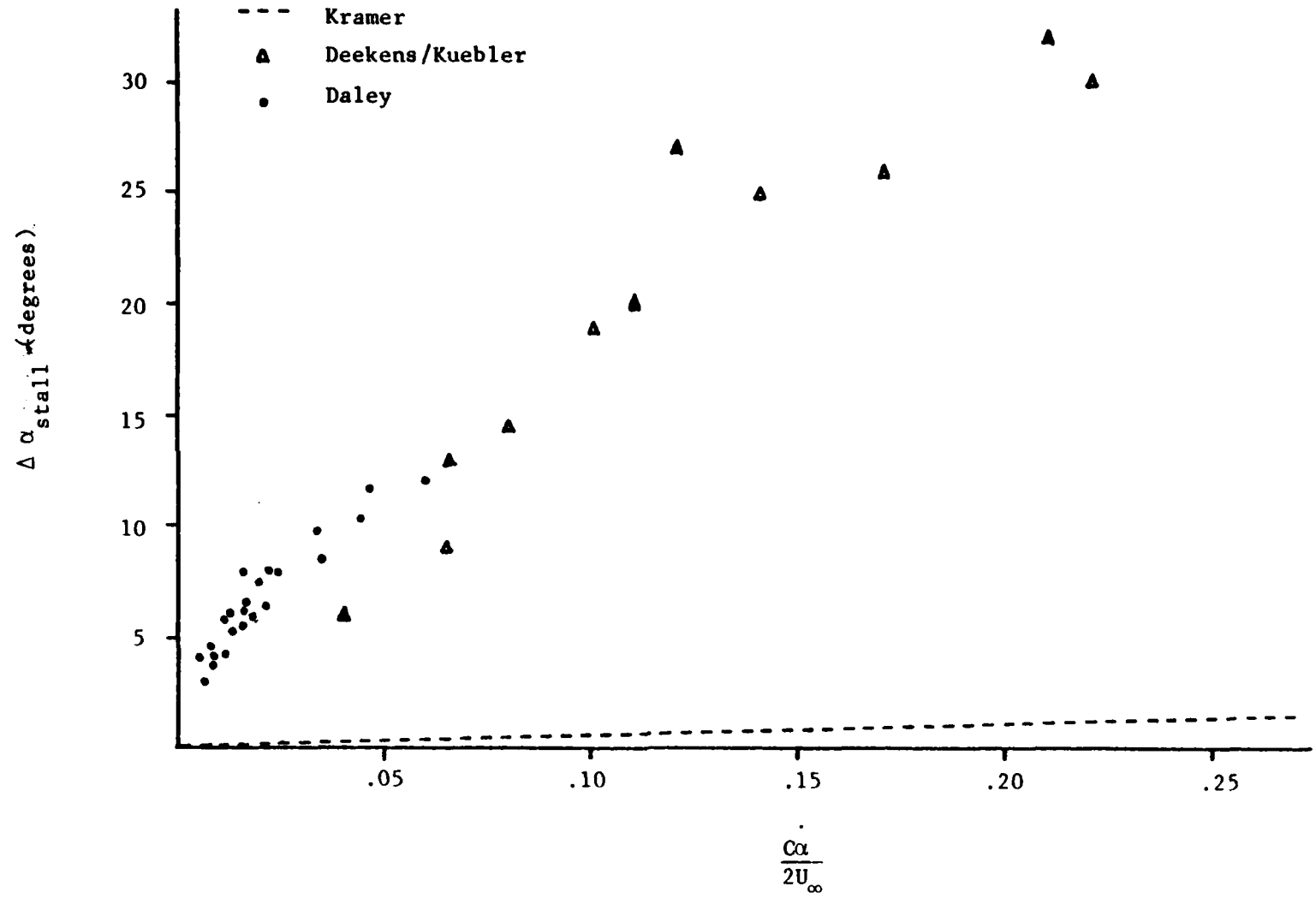

Figure 1. Results of Experimental Investigations of Dynamic Stall by Kramer, Deekens/Kuebler, and Daley

II. Gust Response Problem

Review of Docken's Work

It is notable that in Docken's approach to the problem of gust response, each step of this theory development and development of the method of integration is simply an unsteady modification of the corresponding steady flow model (Ref 6:17,20). This idea is reinforced by the fact that, when his program is applied to a case of zero pitch rate, time derivatives become zero, and all equations and the resulting solution reduce to the steady-state case.

The theory development leading to the unsteady boundary layer momentum-integral equation is reviewed in Appendix A. In short, the principles of continuity and momentum are applied to an incremental control volume in the boundary layer. The unsteady Euler's equation is then employed to substitute for the pressure gradient term. By careful manipulation of terms, the momentum-integral equation for unsteady flow results:

$$\frac{\partial}{\partial x} U_e^2 \int_0^h \frac{u}{U_e}\left(1 - \frac{u}{U_e}\right)dy + U_e \frac{\partial U_e}{\partial x} \int_0^h \left(1 - \frac{u}{U_e}\right)dy$$

$$+ \frac{\partial}{\partial t} U_e \int_0^h \left(1 - \frac{u}{U_e}\right)dy = \frac{\tau_w}{\rho} \qquad (1)$$

Docken's modification to the von Karman-Pohlhausen integral method to handle unsteady flow is reviewed in Appendix B. As in the well known steady flow model (Ref 7:158-160), the displacement thickness and momentum thickness are substituted into the momentum-integral equation. The velocity

profile is defined as a polynomial expression of y/δ, and, by applying known boundary conditions, the velocity profile can be related to a single shape parameter:

$$\Lambda = \frac{\delta^2}{\nu} \left(\frac{\partial U_e}{\partial x} + \frac{1}{U_e} \frac{\partial U_e}{\partial t}\right) \tag{2}$$

Again as in the steady-flow model, additional parameters are defined and substituted into the governing equation, and the "working" equations for stepwise integration become

$$\frac{dZ}{dx} = \left| F(K) + \left[4 + f_1(K)\right] \frac{Z}{U_e} \frac{\partial U_e}{\partial t} \right| \frac{1}{U_e} \tag{3}$$

and

$$Z = K\left(\frac{\partial U_e}{\partial x} + \frac{1}{U_e} \frac{\partial U_e}{\partial t}\right)^{-1} \tag{4}$$

The single exception to this parallelism of the unsteady flow derivation to the steady flow derivation arises from the introduction of the displacement and momentum thicknesses into the momentum-integral equation. A transient term of the form $\frac{\partial \delta_1}{\partial t}$ developed, requiring a closure equation. The necessary equation was derived as

$$\frac{\partial \delta_1}{\partial t} = -\frac{\delta_1}{2U_e}\frac{\partial U_e}{\partial t} \qquad \text{(Ref 3)} \qquad (5)$$

The limits of applicability of the assumptions associated with this derivation were not investigated in depth, however, and both the derivation and the underlying assumptions will be examined in Section III of this report.

The method used to step-wise numerically integrate Eqs (3) and (4) along the surface of a Joukowski airfoil is detailed in Appendix C. Coordinates on the airfoil and velocity at the outer edge of the boundary layer are obtained by a Joukowski transformation from flow about a circular cylinder, the unsteadiness being approximated as pseudo-steady Joukowski solutions at the changing angles of attack. Necessary derivatives at each step are computed using standard difference methods, and the shape parameter can be examined at any given point on the airfoil to determine a point of boundary layer separation (Ref 6:23-25).

Docken defined aerodynamic stall as the condition of flow separation at the quarter-chord of the airfoil. Flow separation was determined to occur when shear at the airfoil surface equals zero, as indicated by the shape parameter ($\Lambda = -12$, or $K = -.1567$). Using this criteria, the above method of solution was applied to a J015 airfoil. By assuming the C_l-vs.-α slope remains linear and equal to 2π/radian, and applying three-dimensional flow corrections, Docken's analytical results were expressed as

$$\Delta C_{L_{max}} = .343\,\frac{c\dot{\alpha}}{U_\infty}$$

comparing remarkably well with Kramer's experimental results:

$$\Delta C_{L_{max}} = .36 \frac{C\dot{\alpha}}{U_\infty}$$

The significance of this result is not only that an approximate integral method had been modified to give such a degree of accuracy, but that, like the experimental results, the relationship between gust pitch rate and dynamic stall angle of attack is linear (Ref 6:27). Also, and just as important, the cause of the increased angle of attack can be attributed to a distinct physical effect -- a reduction in the adversity of the pressure gradient as determined from Euler's equation.

Modification and Results

Upon close examination of the Docken program, an error was discovered in the Joukowski transformation. The error was, in fact, causing the method of solution to be applied to an airfoil with thickness less than the desired 15%. This error was corrected and some other minor modifications were made to the original work.

Upon running the solution again for a J015 airfoil, the data remained linear, but with a different linear coefficient. The corrected data is displayed graphically in Figure 2.

Converting this data in order to compare with Kramer's results, the results of Figure 2 may be expressed as

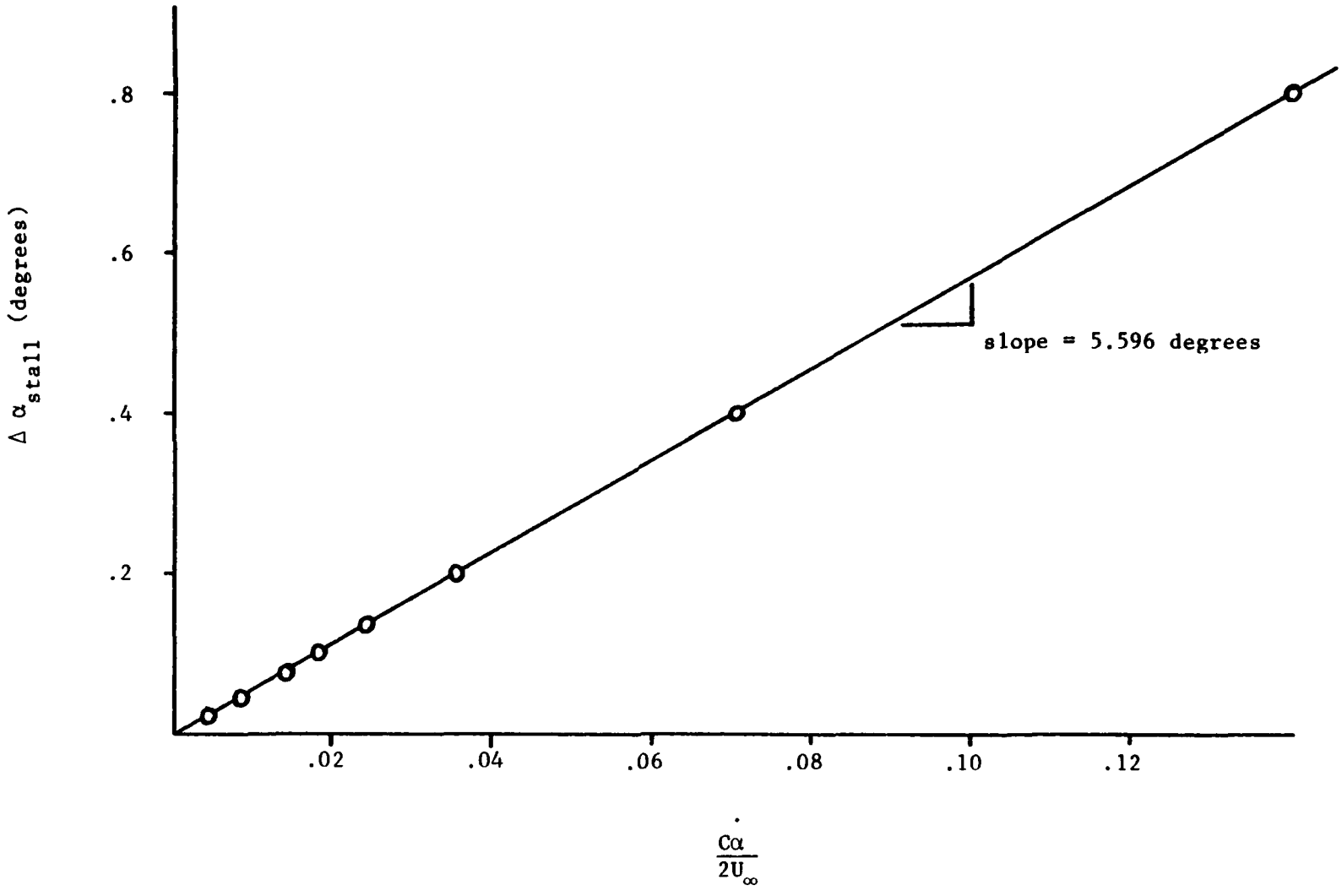

Figure 2. Change in Separation Angle of Attack Due to Gust Response

$$\alpha_{stall(dyn)} = \alpha_{stall(st)} + 5.60 \left(\frac{\dot{C\alpha}}{2U_\infty}\right)$$

In radians then, and correcting the form of the non-dimensional pitch rate,

$$\alpha_{stall(dyn)} = \alpha_{stall(st)} + 0.049 \frac{\dot{C\alpha}}{U_\infty}$$

Assuming, by classical airfoil theory, a 2π/radian curve slope (Ref 8:125),

$$C_{l_{max(dyn)}} = C_{l_{max(st)}} + .307 \frac{\dot{C\alpha}}{U_\infty}$$

Since Kramer's experiment dealt with a wing with aspect ratio approximately equal to five, a three-dimensional flow correction is required. By wing-section theory, the lift curve slope per degree of the corresponding wing may be obtained by

$$C_{L_\alpha} = \frac{C_{l_\alpha}}{1 + \left(\frac{57.3\ C_{l_\alpha}}{\pi\ AR}\right)} \qquad \text{(Ref 9:11)}$$

This, then yields the result

$$\Delta C_{L_{max}} = .220 \frac{C\dot{\alpha}}{U_\infty}$$

This differs somewhat in degree of accuracy, but the solution still exhibits the significance of linearity and physical interpretation, and is still very close to Kramer's empirical results.

III. Closure Equation

Review of Derivation

Prior to Docken's work, the von Karman-Pohlhausen technique had not been used to solve an unsteady flow problem, because the unsteady terms in the momentum-integral equation required an additional unknown closure equation. The derivation of the required equation is simple and concise, and the assumptions appear to be well-founded, at least superficially (Ref 6:14-15). In order to investigate the validity of these assumptions, and hence the equation, and to then further examine the impact on the problem solution, it is necessary first to fully understand the derivation.

To find the equation of closure, it is first observed that, for any location and time in the flow, the displacement thickness is related to the boundary layer thickness as

$$\delta_1 = C_1 \delta \tag{6}$$

Also, for laminar flows, the boundary layer thickness is related to the velocity of the potential flow as

$$\delta = C_2 \left(\frac{\nu}{U_e x}\right)^{1/2} \tag{7}$$

Then, taking the time derivatives of Eqs (6) and (7),

$$\frac{\partial \delta_1}{\partial t} = C_1 \frac{\partial \delta}{\partial t} + \frac{\partial C_1}{\partial t} \delta \tag{8}$$

and

$$\frac{\partial \delta}{\partial t} = - \frac{C_2}{2U_e} \left(\frac{\nu}{U_e x}\right)^{1/2} \frac{\partial U_e}{\partial t} + \frac{\partial C_2}{\partial t} \left(\frac{\nu}{U_e x}\right)^{1/2} \tag{9}$$

Substituting Eqs (7) and (9) into Eq (8) gives

$$\frac{\partial \delta_1}{\partial t} = - \frac{C_1 C_2}{2U_e} \left(\frac{\nu}{U_e x}\right)^{1/2} \frac{\partial U_e}{\partial t} + C_1 \frac{\partial C_2}{\partial t} \left(\frac{\nu}{U_e x}\right)^{1/2}$$

$$+ C_2 \frac{\partial C_1}{\partial t} \left(\frac{\nu}{U_e x}\right)^{1/2} \tag{10}$$

Now, the restrictive assumption is made that the time dependence of both C_1 and C_2 is small compared to that of U_e, and Eq (10) becomes

$$\frac{\partial \delta_1}{\partial t} = - \frac{C_1 C_2}{2U_e} \left(\frac{\nu}{U_e x}\right)^{1/2} \frac{\partial U_e}{\partial t} \tag{11}$$

Applying Eqs (6) and (7) to Eq (11) then yields the required closure equation:

$$\frac{\partial \delta_1}{\partial t} = - \frac{\delta_1}{2U_e} \frac{\partial U_e}{\partial t} \tag{12}$$

Investigation of Assumptions

The key assumption then is that $\frac{\partial C_1}{\partial t}$ and $\frac{\partial C_2}{\partial t}$ are negligibly small, and the question arises as to what magnitudes are acceptable to the solution. From Eqs (10) and (11), it can be seen that the closure equation is valid if

$$- \frac{C_1 C_2}{2U_e} \left(\frac{\nu}{U_e x}\right)^{1/2} \frac{\partial U_e}{\partial t} \simeq - \frac{C_1 C_2}{2U_e} \left(\frac{\nu}{U_e x}\right)^{1/2} \frac{\partial U_e}{\partial t} + C_1 \frac{\partial C_2}{\partial t} \left(\frac{\nu}{U_e x}\right)^{1/2}$$

$$+ C_2 \frac{\partial C_1}{\partial t} \left(\frac{\nu}{U_e x}\right)^{1/2} \tag{13}$$

Then, to compare the relative magnitudes of the time derivatives, Eq (13) requires that

$$\left| \frac{C_1 C_2}{2U_e} \frac{\partial U_e}{\partial t} \right| \gg \left| C_1 \frac{\partial C_2}{\partial t} + C_2 \frac{\partial C_1}{\partial t} \right| \tag{14}$$

From this it can be seen that, while this relationship is certainly satisfied if the original assumption is true, it is also satisfied if the sum, $C_1 \frac{\partial C_2}{\partial t} + C_2 \frac{\partial C_1}{\partial t}$, is comparatively small. This could certainly be the case if the time variations of C_1 and C_2 are of opposite sign.

Either of these assumptions could be evaluated by the degree to which Eq (14) is satisfied. The velocity and acceleration terms are available at any given point on an airfoil by the Pohlhausen method previously discussed; however, a scheme must be developed to determine C_1, C_2, and the corresponding time derivatives.

Consider first the term C_1. By definition, as in Eq (6), C_1 is the ratio of displacement thickness to boundary layer thickness. This can be written in terms of the Pohlhausen velocity profile shape parameter as

$$C_1 = \frac{\delta_1}{\delta} = \frac{3}{10} - \frac{\Lambda}{120} \tag{15}$$

Then the time derivative of C_1, also in terms of the shape parameter, is

$$\frac{\partial C_1}{\partial t} = -\frac{1}{120} \frac{\partial \Lambda}{\partial t} \tag{16}$$

When an airfoil is at an angle of attack such that separation is indicated at the quarter-chord (i.e., the case under consideration), the

shape parameter varies from +7.052 at the stagnation point to -12.0 at quarter-chord (Ref 7:211); hence, $\frac{d\Lambda}{dx}$ for a static airfoil and $\frac{D\Lambda}{Dt}$ for a pitching airfoil are negative quantities. The fact that a pitching airfoil demonstrates delayed separation would infer that the associated $\frac{\partial\Lambda}{\partial t}$ term is causing Λ to be less negative, thus $\frac{\partial\Lambda}{\partial t}$ is a positive term. If this is indeed the case, then $\frac{\partial C_l}{\partial t}$ is a negative term, by Eq (16).

Since the shape parameter is available in the solution at each point on the airfoil, C_l is easily determined. The term $\frac{\partial\Lambda}{\partial t}$, and consequently $\frac{\partial C_l}{\partial t}$, can be calculated in the following manner. The total change in the shape parameter can be calculated between two given points on the airfoil by both the steady solution (time independent) and the pitching solution (time dependent). For the steady case, $\frac{\partial\Lambda}{\partial t} = 0$. Defining the total derivative as

$$\frac{D\Lambda}{Dt} = \frac{\partial\Lambda}{\partial t} + \frac{\partial s}{\partial t}\frac{\partial\Lambda}{\partial s}$$

let $(\frac{D\Lambda}{Dt})_1$ be approximated by a steady, or time-independent, difference of Λ between two given points in close proximity, and $(\frac{D\Lambda}{Dt})_2$ be approximated by the time-dependent difference between the same two points. Then

$$(\frac{D\Lambda}{Dt})_2 - (\frac{D\Lambda}{Dt})_1 = (\frac{\partial\Lambda}{\partial t} + \frac{\partial s}{\partial t}\frac{\partial\Lambda}{\partial s}) - (0 + \frac{\partial s}{\partial t}\frac{\partial\Lambda}{\partial s}) = \frac{\partial\Lambda}{\partial t}$$

Consider now the term C_2. If the velocity of the potential flow over a wedge is proportional to a power of the length coordinate as

$$U(x) = kx^m \tag{18}$$

where m is a specific function of the included wedge angle, then the solutions of Falkner and Skan show that for any given wedge there is a constant C_2 such that

$$\delta = C_2 \left(\frac{\nu}{U_e x}\right)^{1/2} \qquad \text{(Ref 7:164-166)} \tag{19}$$

The constant C_2 is only a function of the geometry; i.e., wedge angle. Comparing Eqs (7) and (19), it can be seen that if such self-similar solutions can be applied to an airfoil approximated by a series of panels (i.e., the wing is made up of a series of short linear ramps), each making a specific "wedge angle" with the free-stream, then C_2 could be determined. Further, since C_2 is only a function of geometry, $\frac{\partial C_2}{\partial t}$ on a pitching airfoil could also be determined through the change in slope of the panel relative to the free-stream over an increment of time.

Accuracy of Closure Equation

Evaluation of the closure equation assumptions was accomplished through

the determination of C_1, C_2, $\frac{\partial C_1}{\partial t}$, and $\frac{\partial C_2}{\partial t}$ on a typical pitching airfoil as it approached separation at the quarter-chord. Using the unsteady Pohlhausen method, U_e, $\frac{\partial U_e}{\partial t}$, and Λ are readily available. An independent set of Falkner-Skan solutions was computed, and a curve fit of the results made, such that the constant C_2 could be determined for any included wedge angle. This and the techniques described in the previous paragraphs were then incorporated into the computer solution, such that at each point on the airfoil a comparison could be made of all of the above terms. Further, each of the following relationships was computed, and a comparison made:

$$-\frac{C_1 C_2}{2U_e}\frac{\partial U_e}{\partial t} \tag{20a}$$

$$-\frac{C_1 C_2}{2U_e}\frac{\partial U_e}{\partial t} + C_1\frac{\partial C_2}{\partial t} + C_2\frac{\partial C_1}{\partial t} \tag{20b}$$

From Eq (13) it can be seen that the degree to which the computed value of (20a) approaches that of (20b) is representative of the accuracy of the closure equation.

Investigation was made of eight separate cases, each varying in free-stream velocity and pitch rate, such that non-dimensional pitch rates varied from .009 to .035. The following observations were made:

a. $\frac{\partial C_1}{\partial t}$ and $\frac{\partial C_2}{\partial t}$ are indeed smaller than $\frac{\partial U_e}{\partial t}$, but not negligibly so. The magnitudes of $\frac{\partial C_1}{\partial t}$ and $\frac{\partial C_2}{\partial t}$ increase

with increasing chord position, while $\frac{\partial U_e}{\partial t}$ is initially increasing, then decreasing. The ratio of $\frac{\partial U_e}{\partial t} : \frac{\partial C_2}{\partial t} : \frac{\partial C_1}{\partial t}$ varied from $10^4:10^2:1$ to 30:15:1, the latter (worst) case occurring at the quarter-chord (separation point) for the situation of slow free-stream velocity and slow pitch rate.

b. $\frac{\partial C_1}{\partial t}$ was negative in value, while C_1, C_2, and $\frac{\partial C_2}{\partial t}$ were positive. The products $C_1 \frac{\partial C_2}{\partial t}$ and $C_2 \frac{\partial C_1}{\partial t}$ then had a canceling effect on one another.

c. The comparison of terms (20a) and (20b) is shown in Figure 3 and was nearly identical for all test cases. This would indicate an accuracy of the closure equation as reflected in Figure 4.

It may be noted here that the validity of the method used to determine C_2 and $\frac{\partial C_2}{\partial t}$ is in question, since it is not known if the velocity on the airfoil taken from Joukowski transformation agrees with Eq (18). To investigate this, a program was written to simultaneously and independently compute two velocities on a representative pitched airfoil. One velocity was that obtained from the Joukowski transformation, while the other began with an identical value at the leading edge of the airfoil and progressed over a series of incremental panels (representative of wedges of identical slope to the airfoil as discussed earlier). This was done using Eq (18), where x is the additive distance traversed over the panels from the

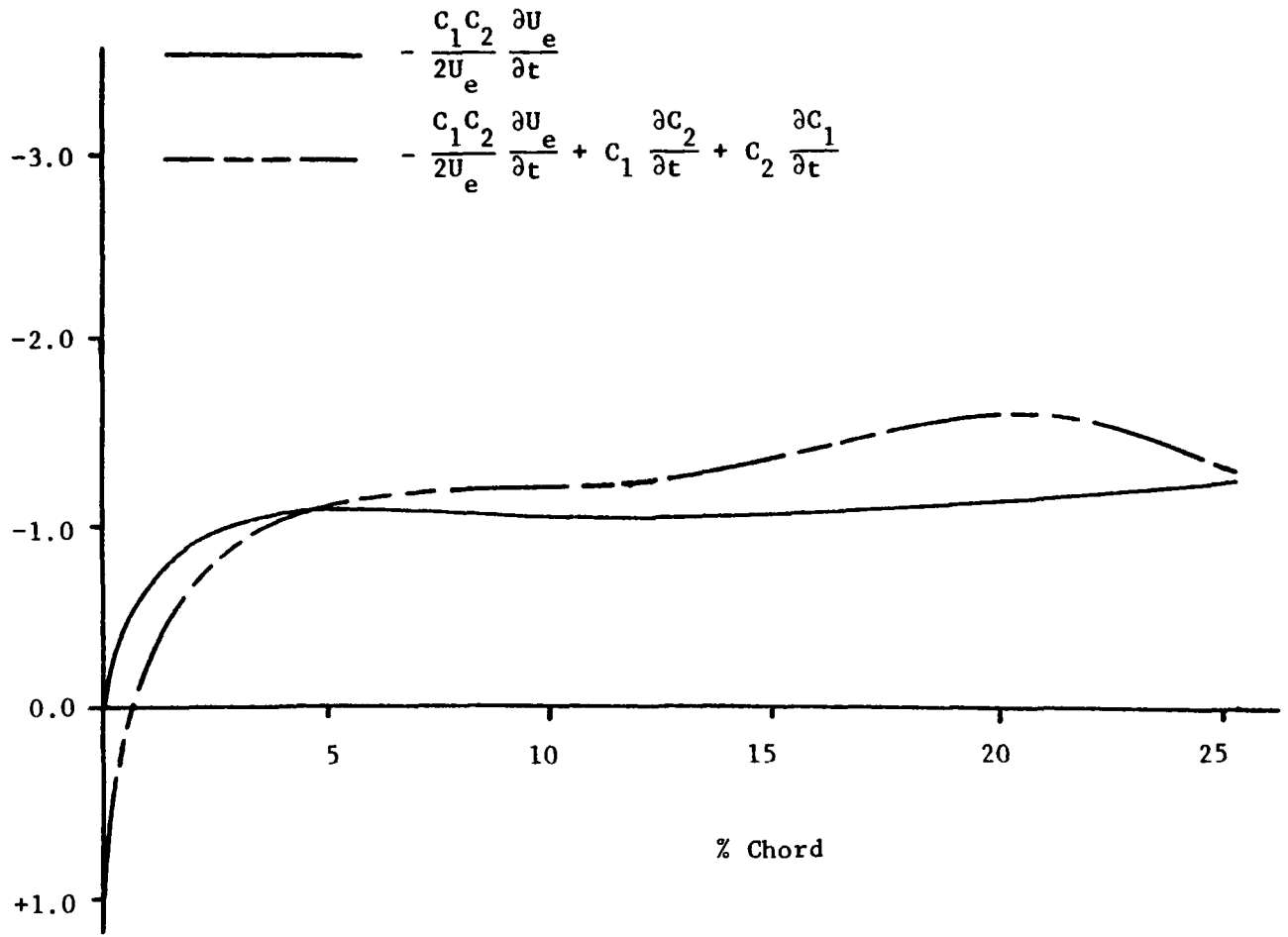

Figure 3. Comparison of Predicted and Assumed Values for the Closure Equation Term, $\frac{\partial \delta_1}{\partial t}\left(\frac{\nu}{U_e x}\right)^{-1/2}$

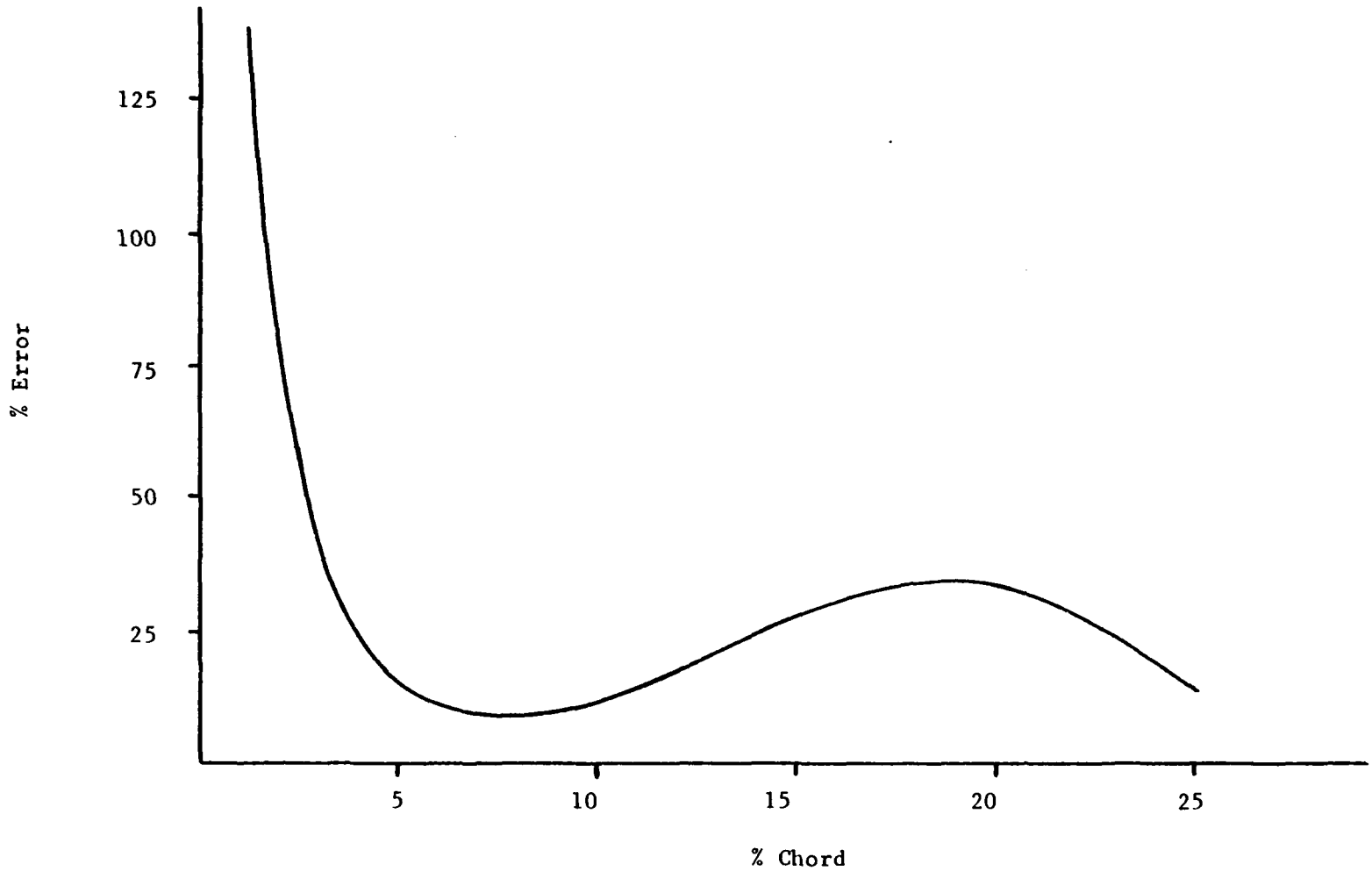

Figure 4. Accuracy of Closure Equation Assumptions

stagnation point and m is determined from the slope of the panel relative to the free-stream. The relationship is

$$m = \frac{\gamma}{2 - \gamma} \qquad \text{(Ref 7:155)}$$

where $\gamma\pi$ is the included angle of the wedge. The constant k can be determined for each panel at the initial juncture by letting U_e at the end of one panel equal U_e at the beginning of the next. Thus, for a juncture of panels i and i + 1 at position x_0

$$k_{i+1} = k_i \left(\frac{x_0^{m_i}}{x_0^{m_{i+1}}} \right)$$

The results of this study are shown in Figure 5. The "panel" velocity varied in error from 6% (negative) near the leading edge to 15% (positive) at the quarter-chord. The velocities were nearly identical in the vicinity of .05 chord.

Consider the hypothetical effect of forcing the panel-derived velocities to agree with the Joukowski-derived velocities. This would require "wedge" panels with an increased included angle near the leading edge, and a decreased included angle aft of about .05 chord. The effect would be to reduce the value of C_2 and $\frac{\partial C_2}{\partial t}$ forward of .05 chord, and increase the values aft of .05 chord.

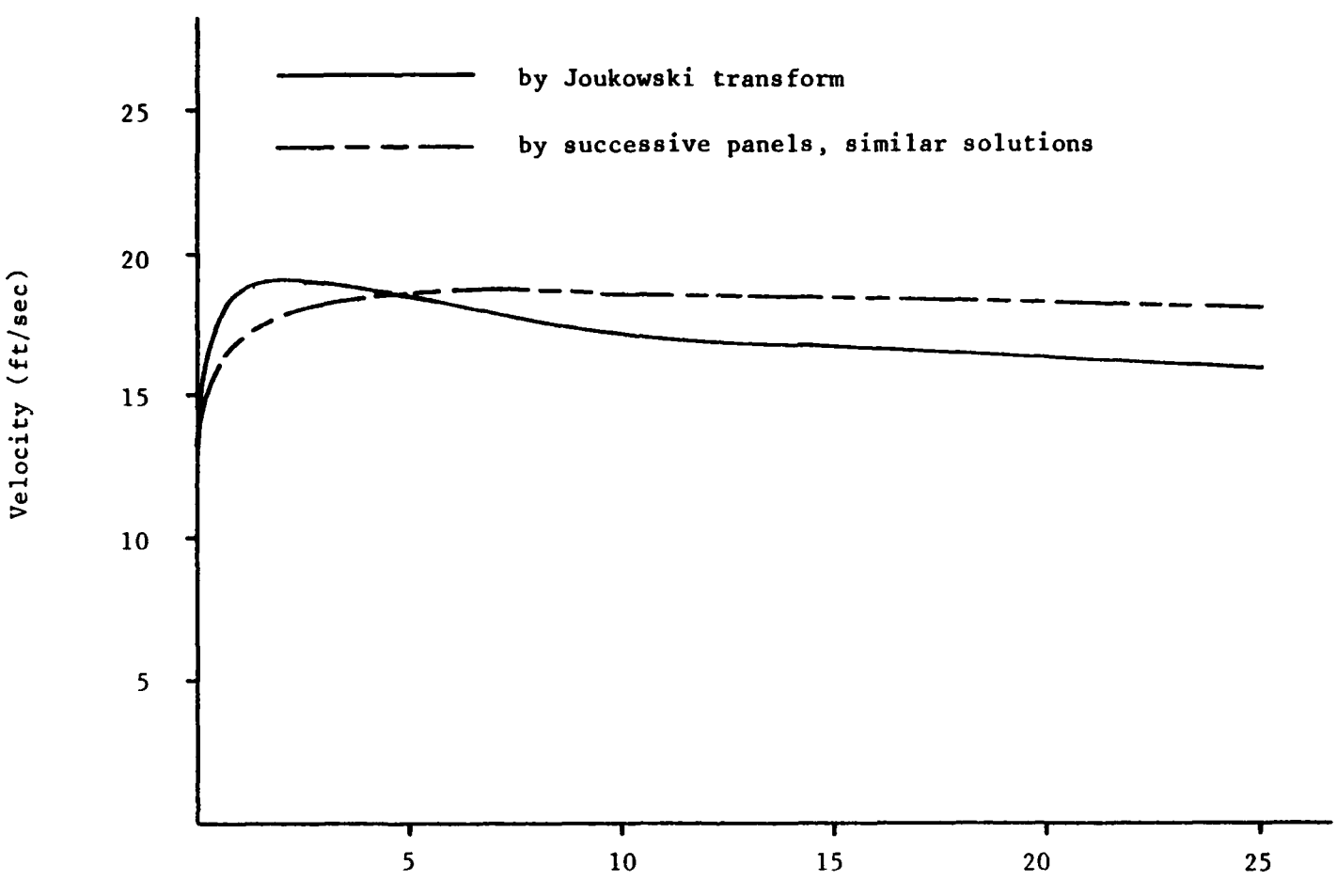

Figure 5. Comparison of Potential Velocities on the Surface of an Airfoil

Now consider the effect on the results of Figure 3. It can be shown that $\frac{\partial C_2}{\partial t}$ is affected considerably more than C_2 by any change in the included angle. Then the end effect would reduce the relative error of the closure equation everywhere on the airfoil. Note also that Figure 3 indicates that the closure equation, like the above velocities, has near zero error in the vicinity of .05 chord.

In order to determine the effect that error in the closure equation has on the prediction of dynamic change in stall angle of attack, errors of 50% (very conservative, as shown in Figure 3) and 25% (more realistic but still conservative as argued above) were introduced into Eq (12). The unsteady Pohlhausen equations were then derived in the same manner used by Docken. The results are that a 50% error in the closure equation results in a 13.54% under-prediction of the dynamic effect on stall angle of attack, and 25% error in the closure equation results in under-predicting this effect by 7.04%. The error presented then in the closure equation has kept the final results on the conservative side and shows that the closure equation is a good one, but for slightly different reasons than stated by Docken.

IV. Further Investigation of Gust Response

Better Match of Kramer's Airfoils

In a closer examination of Kramer's experimental work, it may be noted that data was taken from two considerably different airfoil profiles -- a Göttingen 459 (symmetric) airfoil and a Göttingen 398 (cambered) airfoil. The resulting dynamic effects on maximum coefficient of lift were almost identical, and Kramer states that the profile of the wing apparently has little influence (Ref 2).

The nature of the unsteady solution method developed by Docken readily lends itself to an investigation of this hypothesis. To this end, a simple computer program was written to determine what specific input data were necessary to reproduce desired variations in thickness and camber to a Joukowski airfoil. It was found that a 12.64% thick symmetrical airfoil very closely matched the Göttingen 459 airfoil in shape, and a Joukowski airfoil with 13.72% thickness and 3.17% camber likewise closely matched the Göttingen 398 airfoil. A comparison of airfoil shapes is shown in Figure 6 and 7.

After a minor modification to the Docken program to allow for camber variation, computer solutions were obtained for maximum angle of attack of each of the above airfoils. Nine sets of conditions were run for each airfoil, and the results are shown in Figure 8.

The results, when converted as in Section II to compare with Kramer's data, are as follows:

For the Göttingen 459 (symmetric) airfoil:

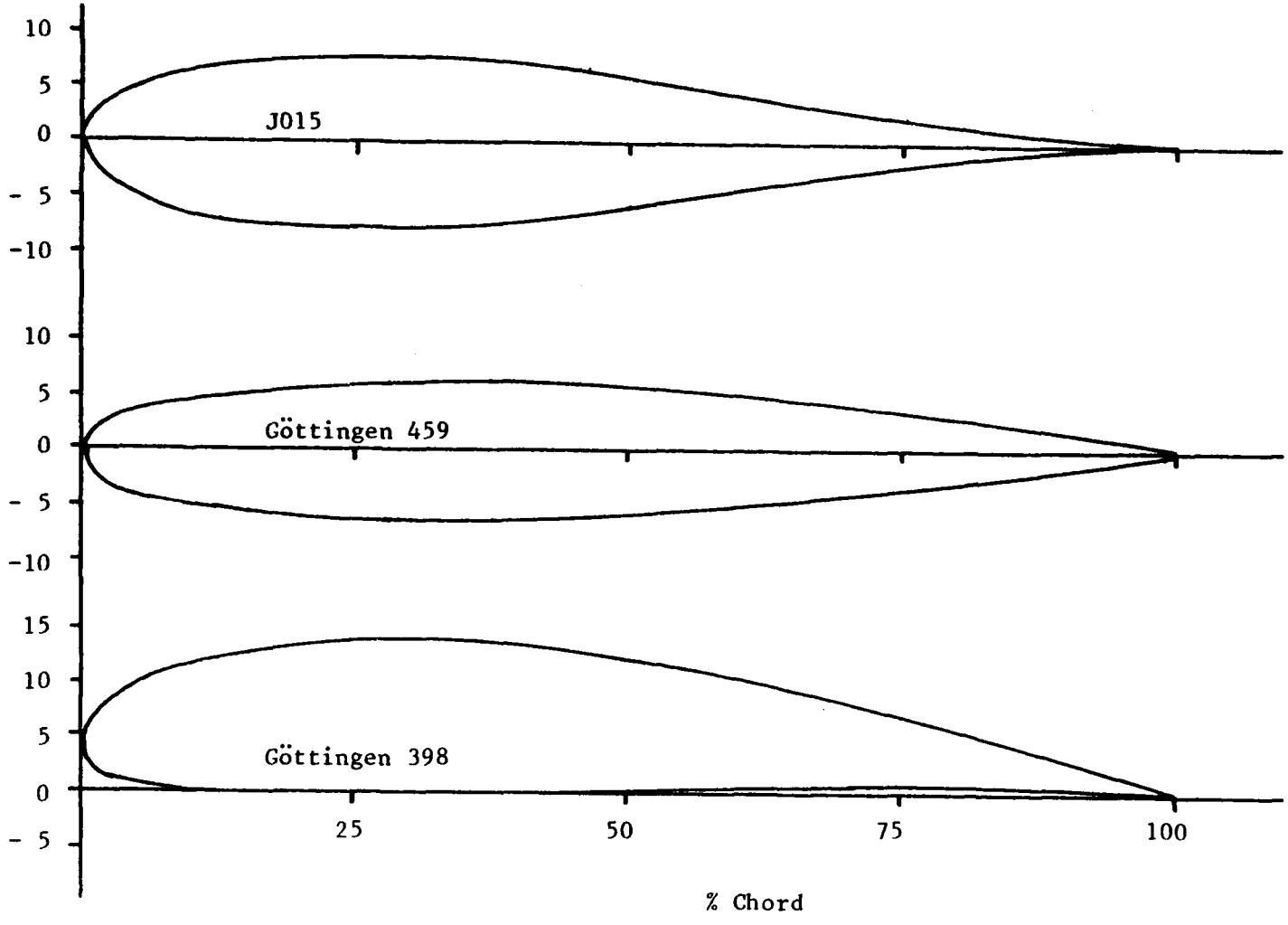

Figure 6. Comparison of Airfoil Shapes Used by Kramer

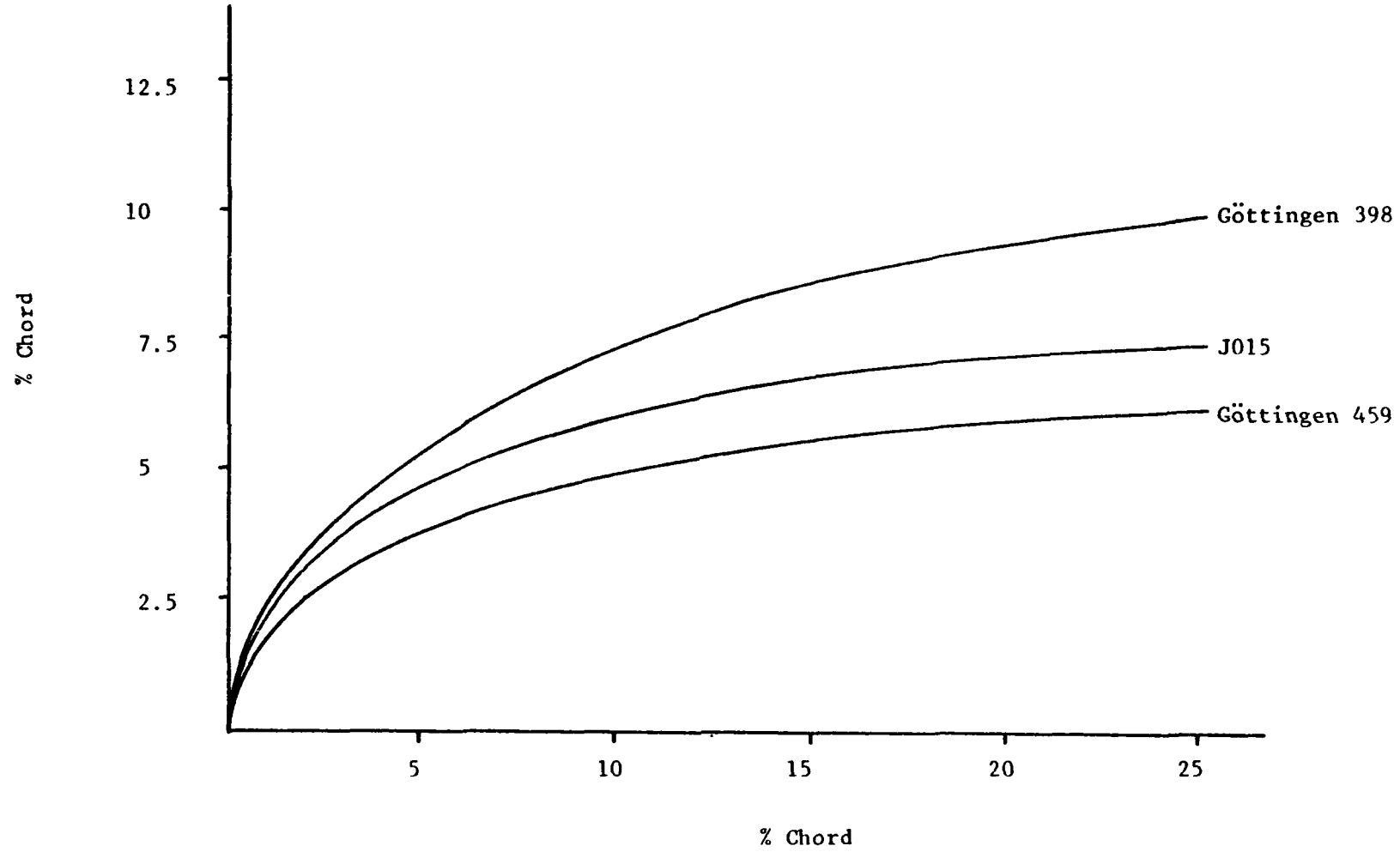

Figure 7. Comparison of Upper-Surface Profiles,
From Leading Edge to Quarter-Chord

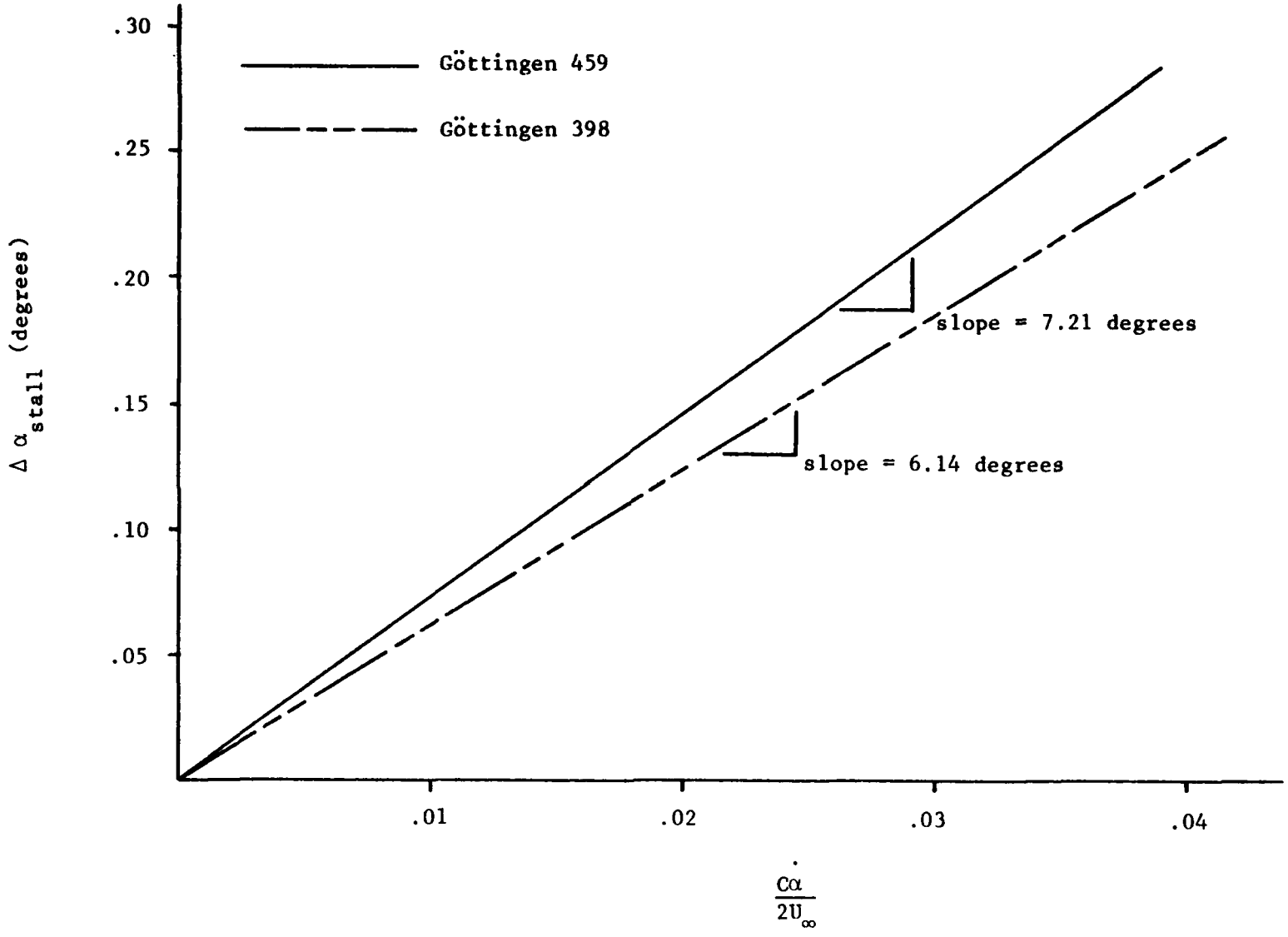

Figure 8. Change in Separation Angle of Attack
Due to Gust Response for Göttingen Airfoils

$$\Delta C_{L_{max}} = \begin{cases} .396 \dfrac{C\dot{\alpha}}{U_\infty} \\ \text{or} \\ .283 \dfrac{C\dot{\alpha}}{U_\infty} \quad \text{corrected for } \mathrm{AR} = 5 \end{cases}$$

For the Göttingen 398 (cambered) airfoil:

$$\Delta C_{L_{max}} = \begin{cases} .337 \dfrac{C\dot{\alpha}}{U_\infty} \\ \text{or} \\ .241 \dfrac{C\dot{\alpha}}{U_\infty} \quad \text{corrected for } \mathrm{AR} = 5 \end{cases}$$

For comparison, recall that Kramer's experimental results for each of the above airfoil profiles were

$$\Delta C_{L_{max}} = .36 \frac{C\dot{\alpha}}{U_\infty}$$

And for Docken's J015 airfoil:

$$\Delta C_{L_{max}} = \begin{cases} .307 \dfrac{C\dot{\alpha}}{U_\infty} \\ \text{or} \\ .220 \dfrac{C\dot{\alpha}}{U_\infty} \quad \text{corrected for } \mathrm{AR} = 5 \end{cases}$$

Note that with the better Joukowski shape approximation of the Göttingen airfoils, results were considerably closer to Kramer's solution. It is meaningless to discuss relative error between any of the computer results and Kramer's experimental results because of the assumptions inherent to the momentum-integral method of solution and approximations necessary to compare results; however, the proximity of the above solutions

is certainly remarkable. Note also that the profile of the airfoil did, in fact, affect the results.

Thickness and Camber Effects

Kramer discusses measurements only on wings with profiles of the two airfoils examined here, and apparently bases his assumption that profile has little effect only on those results. From Figure 8 it can be seen that these particular airfoils do not differ much in change of stall angle of attack, even though the airfoil shapes are considerably different. The fact that there does exist a difference based on shape alone, however, suggests further investigation is in order.

Two studies were conducted regarding airfoil shape. First, using a symmetrical Joukowski airfoil, the thickness was varied, with a linear coefficient of increase of stall angle of attack per non-dimensional pitch rate being calculated for maximum thicknesses of 10%, 12.68%, 15%, 20%, and 25%. Secondly, a 15% thick Joukowski airfoil was varied in camber, and the same coefficient calculated for maximum cambers of 0%, 1%, 2.5%, 5%, and 7.5%. The results are displayed graphically in Figures 9 and 10, respectively.

The dynamic stall effect was decreased as airfoil thickness increased and as camber increased. While camber has a relatively slight effect, the thickness effect was dramatic. It would appear then that airfoil profile is indeed an important factor in dynamic stall effect. It should be noted that, while Kramer's airfoils appear very different, they differ by only about 1% in maximum thickness.

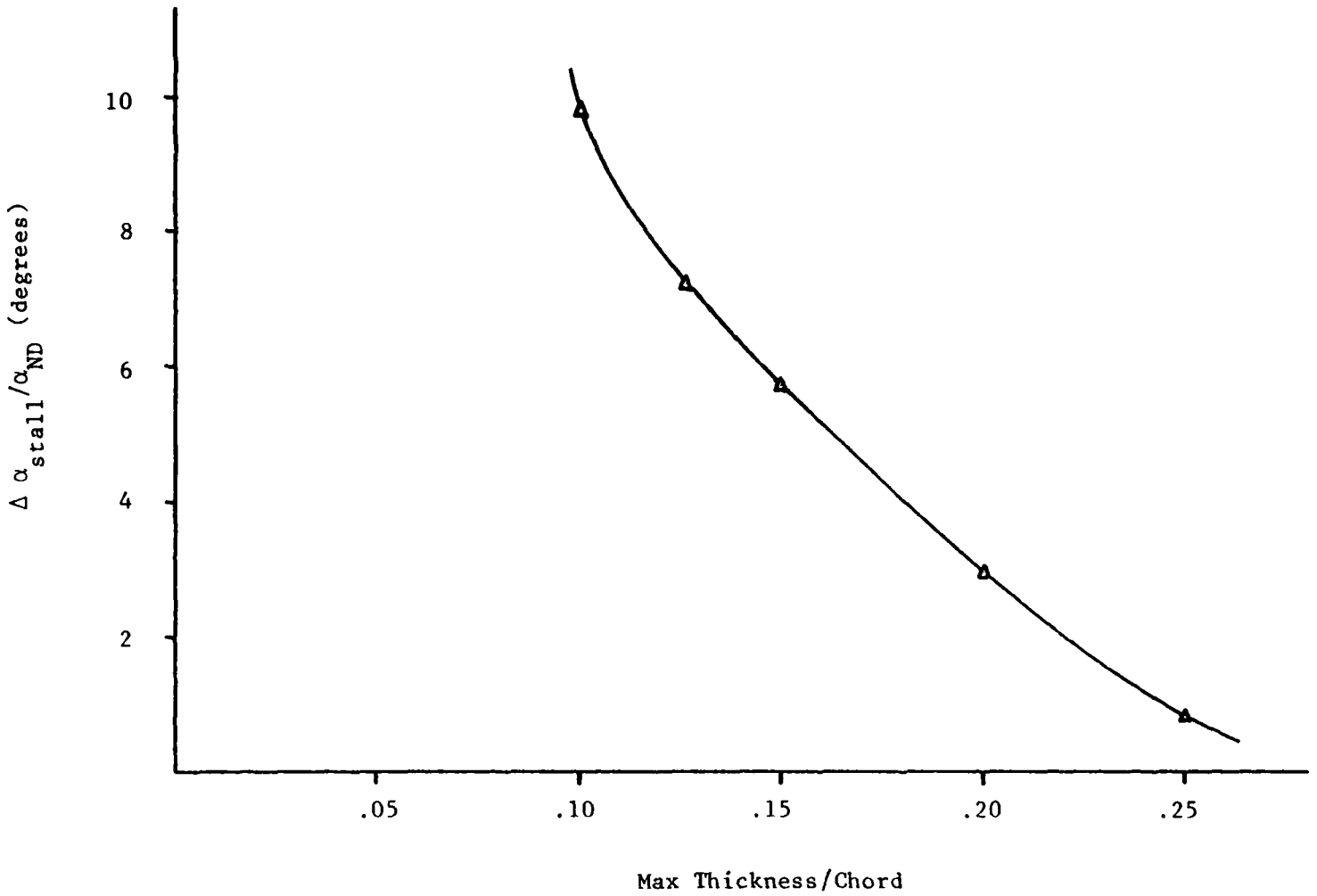

Figure 9. Effect of Airfoil Thickness on Gust Response Solution

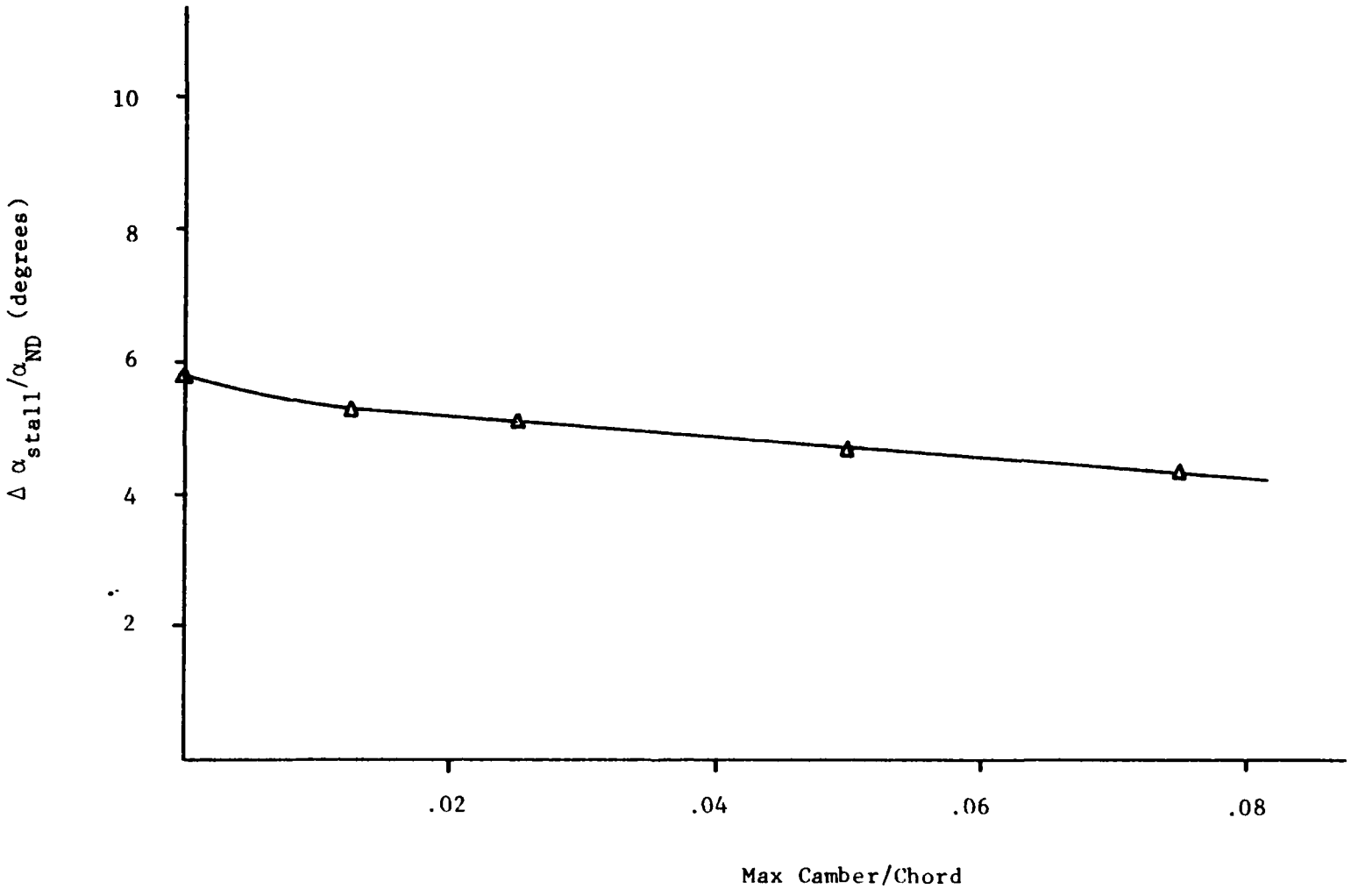

Figure 10. Effect of Airfoil Camber on Gust Response Solution

V. Pitching Airfoil Problem

Non-Inertial Control Volume Analysis

As discussed previously, the only readily apparent difference between the gust-response problem and the pitching airfoil problem is the frame of reference. It was anticipated that, due to the similarity of these problems, it may be possible to investigate the dynamic stall effects on a pitching airfoil by paralleling the approach taken in the gust-response solution. The procedure then is to derive a momentum-integral equation for the boundary layer by developing the continuity and momentum equations for a fluid element in the boundary layer.

The continuity equation presents no problems. In exactly the same analysis as for the gust-response solution, the principle of continuity is applied to an incremental control volume, with the resulting equation (see Appendix A):

$$\dot{m}_{top} = -\frac{\partial}{\partial x}\int_0^h \rho u dy dx \tag{21}$$

In order to use the momentum equation on this control volume, however, certain modifications must be made. The momentum equation, derived from Newton's Second Law, is usually applied to a control volume that is either fixed, or translating at constant velocity, with respect to an inertial reference frame. The surface of the pitching airfoil, and thus the attached control volume in the boundary layer, is neither. By an analysis

of particle dynamics, certain "hypothetical body forces" can be determined which account for the non-Newtonian motion of the control volume, and with the addition of these forces the control volume analysis may proceed as if it were fixed in inertial space (Ref 10:109-114). The derivation and examination of the hypothetical body forces is included in Appendix D. These body forces in the x-direction are:

$$dB = - dm \left[\beta_1 + \beta_2 v - \beta_3 x \right]$$

where:

$$\beta_1 = R\dot{\alpha}^2 \cos \phi \ ,$$

$$\beta_2 = 2\dot{\alpha} \ ,$$

$$\beta_3 = \dot{\alpha}^2$$

and R is the length from the point of rotation of the airfoil to a reference point in the control volume, and ϕ is the angle between line R and the local surface tangent of the airfoil.

Now referring to Figure 11, the sum of the forces in the x-direction can be equated to the net rate of transport of momentum out of the control volume plus the flux of momentum in the control volume, such that:

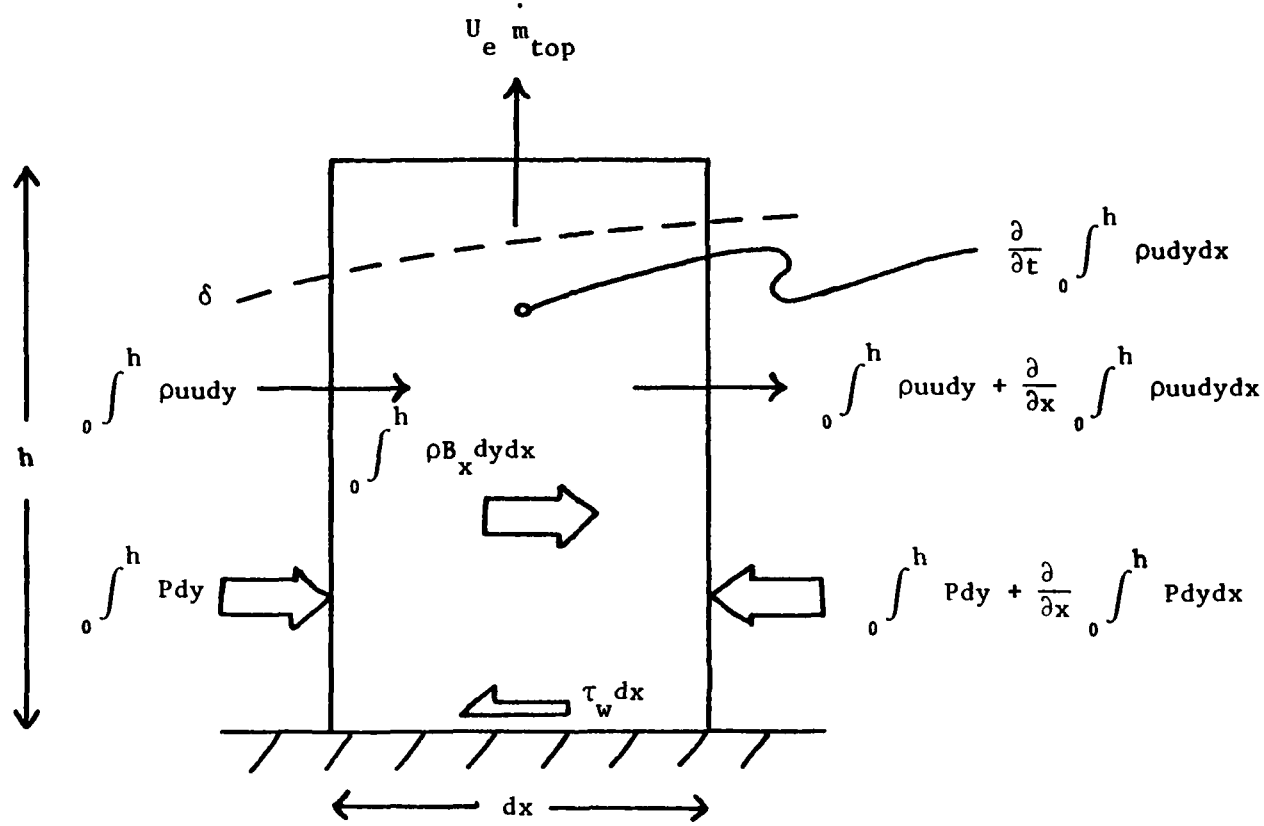

Figure 11. Momentum Conservation in a Non-Inertial Boundary Layer Control Volume

$$\frac{\partial}{\partial x}\int_0^h \rho u u dy dx + U_e \dot{m}_{top} + \frac{\partial}{\partial t}\int_0^h \rho u dy dx =$$

$$-\frac{d}{dx}\int_0^h p dy dx - \tau_w dx - (\beta_1 - \beta_3 dx)\int_0^h \rho dy dx$$

$$- \beta_2 \int_0^h \rho v dy dx \qquad (22)$$

Note that the classical boundary layer assumption is made that a pressure gradient exists only in the x-direction. If Eq (21) is now substituted into (22), and dividing by ρdx, the result is

$$\int_0^h \frac{\partial(uu)}{\partial x} dy - U_e \int_0^h \frac{\partial u}{\partial x} dy + \frac{\partial}{\partial t}\int_0^h u dy =$$

$$-\frac{1}{\rho}\int_0^h \frac{dp}{dx} dy - \frac{\tau_w}{\rho} - (\beta_1 - \beta_3 dx)\int_0^h dy - \beta_2 \int_0^h v dy \qquad (23)$$

Consider the hypothetical body force terms in Eq (23). $\beta_3 dx$ is very small in comparison to β_1; i.e.,

$$\dot{\alpha}^2 dx \ll R \dot{\alpha}^2 \cos \phi$$

It can be shown that R cos ϕ is a large term except very near the leading edge. On the airfoil under consideration, R cos $\phi > 1$ for chord positions between .006 and .250. Since $dx \ll 1$, it may be assumed that

$$(\beta_1 - \beta_3 dx) \int_0^h dy \simeq \beta_1 \int_0^h dy$$

It is demonstrated in Appendix D that a potential flow velocity close to and tangent to the airfoil surface, and of magnitude U^* as observed in the inertial frame of reference, will appear to an observer fixed in the control volume as

$$\bar{U} = (U^* - R\dot{\alpha} \sin \phi)\hat{x} - (R\dot{\alpha} \cos \phi)\hat{y} \qquad (24)$$

Note that there is a constant y-component of velocity toward the surface of the airfoil; but if the surface is impermeable, then this component is necessarily zero at y = 0. Since this difference must be compensated for in the boundary layer, it is assumed that this y-component of velocity is a linear function for $0 \leq y \leq \delta$. Then

$$v = -\frac{R\dot{\alpha} \cos \phi}{\delta} y, \qquad y \leq \delta$$

and

$$v = - R \dot{\alpha} \cos \phi , \qquad y > \delta$$

Now,

$$- \beta_1 \int_0^h dy - \beta_2 \int_0^h v dy = - R \dot{\alpha}^2 \cos \phi \left[\int_0^\delta dy + \int_\delta^h dy \right]$$

$$- 2 \dot{\alpha} \left[\int_0^\delta \left(- \frac{R \dot{\alpha} \cos \phi}{\delta} \right) y dy + \int_\delta^h (- R \dot{\alpha} \cos \phi) dy \right]$$

Carrying out the integrations, this reduces to

$$- \beta_1 \int_0^h dy - \beta_2 \int_0^h v dy = (h - \delta) R \dot{\alpha}^2 \cos \phi$$

The total effect of the hypothetical body forces on a control volume where the upper limit is the edge of the boundary layer ($h = \delta$) is zero. Although at this point h is still arbitrary, the boundary conditions will eventually be applied at $y = \delta$, therefore these terms may be dropped from Eq (23). In the interest of argument, the effect of these terms does not disappear if v does not vary linearly in the boundary layer. Cases

of parabolic and elliptic variations were investigated, with the resulting (small) terms being carried completely through the Pohlhausen derivation and then applied to an airfoil. The effects on the final solution were negligible in both cases.

Eq (23) thus becomes:

$$\int_0^h \frac{\partial(uu)}{\partial x}\,dy - U_e \int_0^h \frac{\partial u}{\partial x}\,dy + \frac{\partial}{\partial t}\int_0^h u\,dy =$$

$$-\frac{1}{\rho}\int_0^h \frac{dP}{dx}\,dy - \frac{\tau_w}{\rho} \qquad (25)$$

At this point the unsteady Euler's equation is used to substitute for the unknown pressure gradient. Letting an asterisk denote velocity as viewed from the inertial reference frame,

$$U_e^* \frac{\partial U_e^*}{\partial x} + \frac{\partial U_e^*}{\partial t} = -\frac{1}{\rho}\frac{dP}{dx} \qquad (26)$$

From Eq (24), an observer in the control volume will see a magnitude of:

$$U_e \simeq U_e^* - R\dot{\alpha}\sin\phi$$

and

$$\frac{\partial U_e}{\partial x} = \frac{\partial U_e^*}{\partial x}, \qquad \frac{\partial U_e}{\partial t} = \frac{\partial U_e^*}{\partial t}$$

Therefore, in terms of the velocity seen by the control volume, Eq (26) becomes

$$(U_e + R\dot{\alpha} \sin \phi) \frac{\partial U_e}{\partial x} + \frac{\partial U_e}{\partial t} = -\frac{1}{\rho} \frac{dP}{dx} \tag{27}$$

Substituting equation (27) for the pressure gradient in Eq (25) yields

$$\int_0^h \frac{\partial(uu)}{\partial x} dy - U_e \int_0^h \frac{\partial u}{\partial x} dy + \frac{\partial}{\partial t} \int_0^h u dy$$

$$= \int_0^h U_e \frac{\partial U_e}{\partial x} dy + R\dot{\alpha} \sin \phi \int_0^h \frac{\partial U_e}{\partial x} dy$$

$$+ \int_0^h \frac{\partial U_e}{\partial t} dy - \frac{\tau_w}{\rho} \tag{28}$$

With the exception of the (added) second term on the right-hand side of this equation, it is exactly the same as that derived for the gust-response problem, and these terms may be manipulated as shown in Appendix A. The resulting modified momentum-integral equation is

$$R\dot{\alpha}\sin\phi\int_0^h\frac{\partial U_e}{\partial x}\,dy+\frac{\partial}{\partial x}U_e^2\int_0^h\frac{u}{U_e}\left(1-\frac{u}{U_e}\right)dy$$

$$+U_e\frac{\partial U_e}{\partial x}\int_0^h\left(1-\frac{u}{U_e}\right)dy+\frac{\partial}{\partial t}U_e\int_0^h\left(1-\frac{u}{U_e}\right)dy=\frac{\tau_w}{\rho}\qquad(29)$$

Modification of von Karman-Pohlhausen Method

Again, as with the gust-response problem in Appendix B, this can be written in terms of the displacement and momentum thicknesses. If the integral of the first term is evaluated with the outer edge of the boundary layer as the upper limit, the result is

$$(R\dot{\alpha}\sin\phi)\frac{\partial U_e}{\partial x}\delta+\frac{\partial}{\partial x}(U_e^2\,\delta_2)+U_e\frac{\partial U_e}{\partial x}\delta_1+\frac{\partial}{\partial t}(U_e\delta_1)=\frac{\tau_w}{\rho}$$

Multiplying this equation by $\frac{\delta_2}{\nu U_e}$ gives

$$(R\,\dot{\alpha}\sin\phi)\,\frac{1}{U_e}\,\frac{\partial U_e}{\partial x}\,\frac{\delta}{\delta_2}\,\frac{\delta_2^2}{\nu} + 2\,\frac{\partial U_e}{\partial x}\,\frac{\delta_2^2}{\nu} + U_e\,\frac{\delta_2}{\nu}\,\frac{\partial \delta_2}{\partial x}$$

$$+\,\frac{\partial U_e}{\partial x}\,\frac{\delta_1}{\delta_2}\,\frac{\delta_2^2}{\nu} + \frac{1}{U_e}\,\frac{\partial U_e}{\partial t}\,\frac{\delta_1}{\delta_2}\,\frac{\delta_2^2}{\nu} + \frac{\partial \delta_1}{\partial t}\,\frac{\delta_2}{\nu} \;=\; \frac{\tau_w \delta_2}{\mu U_e}$$

Applying the closure equation (12), and rearranging terms, this may be written as

$$\left(2 + \frac{\delta_1}{\delta_2}\right)\frac{\delta_2^2}{\nu}\left[(R\,\dot{\alpha}\sin\phi)\,\frac{1}{U_e}\,\frac{\partial U_e}{\partial x} + \frac{\partial U_e}{\partial x} + \frac{1}{U_e}\,\frac{\partial U_e}{\partial t}\right]$$

$$-\left(2 + \frac{\delta_1}{\delta_2} - \frac{\delta}{\delta_2}\right)\frac{\delta_2^2}{\nu}\left[(R\,\dot{\alpha}\sin\phi)\,\frac{1}{U_e}\,\frac{\partial U_e}{\partial x}\right] + \frac{U_e \delta_2 \delta_2'}{\nu}$$

$$-\left(2 + \frac{1}{2}\,\frac{\delta_1}{\delta_2}\right)\frac{\delta_2^2}{\nu}\,\frac{1}{U_e}\,\frac{\partial U_e}{\partial t} \;=\; \frac{\tau_w \delta_2}{\mu U_e} \qquad (30)$$

From this point, the derivation of the working equations for the unsteady Pohlhausen method closely resembles that for the gust-response problem as outlined in Appendix B; therefore, only the differences will be highlighted here.

Due to the change in appearance of the unsteady pressure term, the corresponding boundary condition becomes

$$\nu \frac{\partial^2 u}{\partial y^2} = -\left[(R\,\dot{\alpha} \sin \phi) \frac{\partial U_e}{\partial x} + U_e \frac{\partial U_e}{\partial x} + \frac{\partial U_e}{\partial t}\right] \qquad \text{at} \quad y = 0$$

The shape parameters are defined as

$$\Lambda = \frac{\delta^2}{\nu} \left[(R\,\dot{\alpha} \sin \phi) \frac{1}{U_e} \frac{\partial U_e}{\partial x} + \frac{\partial U_e}{\partial x} + \frac{1}{U_e} \frac{\partial U_e}{\partial t}\right]$$

and:

$$K = \frac{\delta_2^2}{\nu} \left[(R\,\dot{\alpha} \sin \phi) \frac{1}{U_e} \frac{\partial U_e}{\partial x} + \frac{\partial U_e}{\partial x} + \frac{1}{U_e} \frac{\partial U_e}{\partial t}\right]$$

Also, an additional function is defined as

$$f_3(K) = \frac{\delta}{\delta_2} = \left(\frac{37}{315} - \frac{\Lambda}{945} - \frac{\Lambda^2}{9072}\right)^{-1}$$

Substitution into Eq (30) yields

$$\left[2 + f_1(K)\right] K - \left[2 + f_1(K) - f_3(K)\right] \frac{Z\, R\, \dot{\alpha} \sin\phi}{U_e} \frac{\partial U_e}{\partial x}$$

$$+ \frac{U_e}{2} \frac{dZ}{dx} - \left[2 + \frac{1}{2} f_1(K)\right] \frac{Z}{U_e} \frac{\partial U_e}{\partial t} = f_2(K)$$

The resulting working equations for stepwise integration are:

$$\frac{dZ}{dx} = \left\{ F(K) + \left[4 + f_1(K)\right] \frac{Z}{U_e} \frac{\partial U_e}{\partial t} + \left[4 + 2f_1(K) - 2f_3(K)\right] \frac{Z\, R\, \dot{\alpha} \sin\phi}{U_e} \frac{\partial U_e}{\partial x} \right\} \frac{1}{U_e} \tag{31a}$$

and

$$Z = K \left[(R\, \dot{\alpha} \sin\phi) \frac{1}{U_e} \frac{\partial U_e}{\partial x} + \frac{\partial U_e}{\partial x} + \frac{1}{U_e} \frac{\partial U_e}{\partial t} \right]^{-1} \tag{31b}$$

Results for Pitching Motion

The existing program for the gust-response solution was modified such that the non-Newtonian motion of the airfoil could be accounted for. Eqs (31a) and (31b) were implemented, which necessitated computation of the new terms $f_3(K)$ and $R\, \dot{\alpha} \sin\phi$. In addition, recall that the velocity U_e and its corresponding derivatives must now be those that are observed

in a frame of reference fixed to the airfoil surface. A subroutine to the initial program was thus written to compute $R\dot{\alpha}\sin\phi$ (geometry dependent) and to correct the Joukowski transformation-derived velocity for motion of the airfoil.

Upon computing the change in maximum angle of attack for various combinations of free-stream velocity and pitch rate and using the separation condition of zero shear stress at the wall, it was found that the results remained linear with respect to non-dimensional pitch rate. The results are shown in Figure 13, being the set of data points labeled "pitching motion". Note that the effect of a pitching airfoil is approximately three times greater than that of an inertially-fixed airfoil in a pitching airflow (gust response). The cause of this increase in angle of attack of separation appears to be due to the effectively reduced velocity of the free-stream by varying amounts, depending on the location on the airfoil. This velocity modification both delays the onset of and relaxes the severity of the adverse pressure gradient.

Moore-Rott-Sears Model and Results

In considering the pitching airfoil as a "moving wall" type of problem, it is also necessary to reevaluate the criteria for determining the point of separation. Up to this point, separation has been assumed to occur when shear at the wall vanishes, which for a static wall is the limit between forward and reverse flows in the boundary layer. For a wall moving in the direction of flow, this is not true (i.e., the flow may obtain a velocity less than the velocity of the wall but greater than zero). The MRS (Moore-Rott-Sears) model provides criteria of separation based

on the velocity profile which will account for motion of the wall (Ref 11:123-126). It defines separation as the condition where both velocity and shear become zero in a singular fashion at some point in the boundary layer, as seen by an observer in the frame of reference of the wall. This condition is illustrated in Figure 12.

A separate program was written to provide a table of values relating a separation Λ (or K) for any given value of U_{wall}/U_e. Then, by computing U_{wall}/U_e at quarter-chord and comparing with this table, the dynamic-stall condition could be determined by iteration until the final Λ matches the indicated tabular Λ. It should be noted that this is only valid for $\Lambda > -17.76$, since the shape parameter K reaches a mathematical minimum at that point (Ref 12:295-296).

Application of this new stall criteria had a considerable effect on the solution. The results are displayed in Figure 13, labeled "MRS model". Note that the dynamic effect on angle of attack is more than twice that using the old criteria, and the total dynamic effect is about seven times that of the gust-response solution. It is also of interest that the change in angle of attack is now no longer linear with non-dimensional pitch rate, but is curved similar to the data in Figure 1; however, the extent of the dynamic effect falls well short of the experimental data.

Mass Introduction and Results

The combined dynamic effects thus far discussed predict an angle of attack change considerably less than experimental results indicate, as shown in Figure 13. This implies that other contributing factors are involved, and it was suggested that mass introduction into the boundary layer may

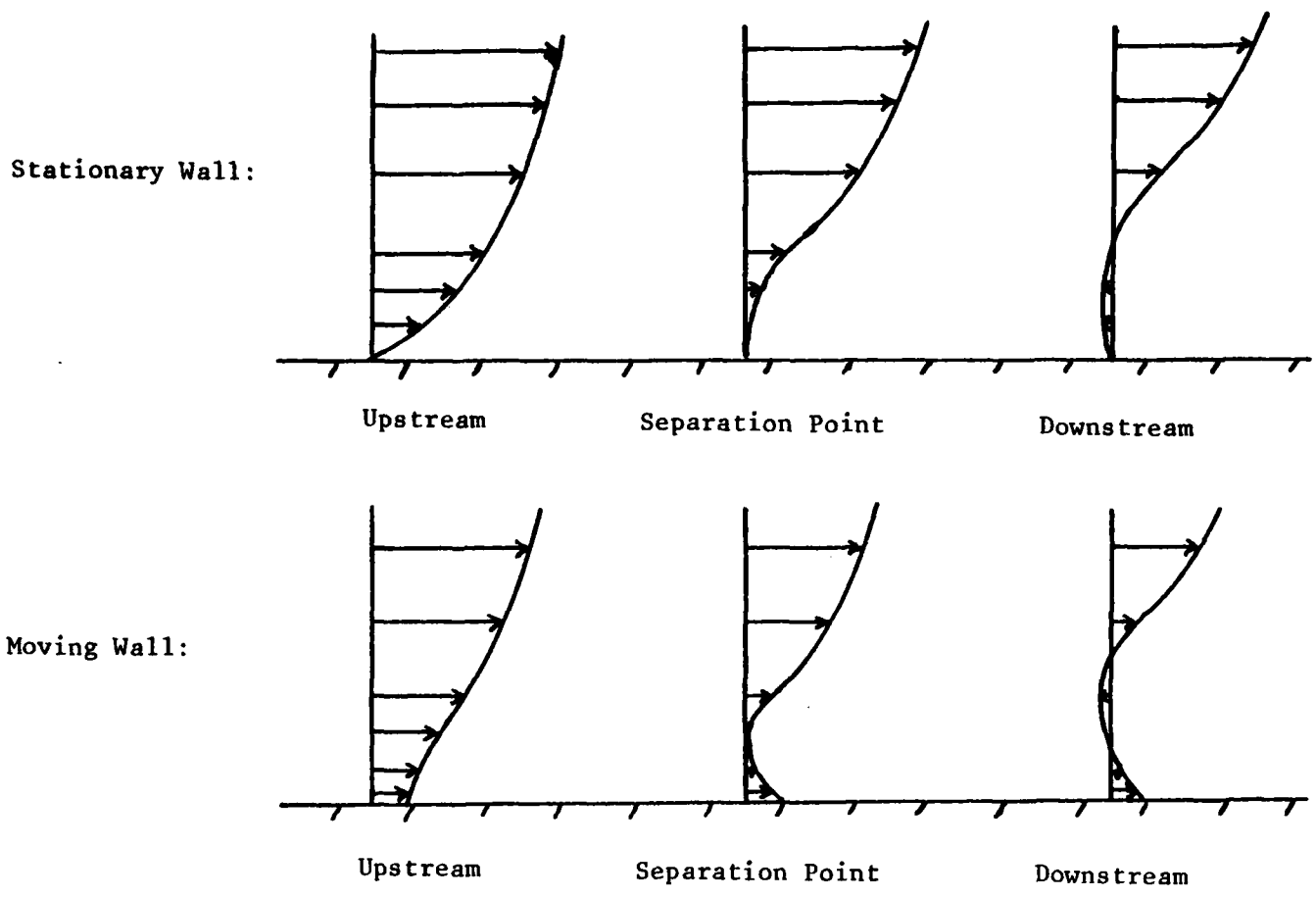

Figure 12. Boundary Layer Velocity Profiles At and Near Separation for a (a) Stationary Wall, and (b) Stream-wise Moving Wall

be a contributing cause. Note that Eq (24) indicates that a potential flow velocity at the edge of the boundary layer does in fact have a component toward the surface when viewed from the control volume. While this normal component is everywhere small, a review of boundary layer solutions involving "suction" and "blowing" indicates that very small mass flow rates can have dramatic effects on boundary layer separation (Ref 7:380-399).

To implement this idea into the method of solution, Eq (21) was amended to account for an additional increment of mass, $C(R\dot{\alpha}\cos\phi)\,dx$, into the top of the control volume (where C is some as yet undetermined constant):

$$\dot{m}_{top} = -\frac{\partial}{\partial x}\int_0^h \rho u dy dx - C(R\dot{\alpha}\cos\phi)\,dx \tag{32}$$

The substitution of this into the momentum equation, with all other terms carried forward as previously described, results in an amended momentum-integral equation:

$$R\dot{\alpha}\sin\phi\int_0^h \frac{\partial U_e}{\partial x}\,dy + \frac{\partial}{\partial x}U_e^2\int_0^h \frac{u}{U_e}\left(1-\frac{u}{U_e}\right)dy$$

$$+ U_e\frac{\partial U_e}{\partial x}\int_0^h \left(1-\frac{u}{U_e}\right)dy + \frac{\partial}{\partial t}U_e\int_0^h \left(1-\frac{u}{U_e}\right)dy$$

$$- C\,U_e(R\dot{\alpha}\cos\phi) = \frac{\tau_w}{\rho} \tag{33}$$

Casting Eq (33) into the Pohlhausen form as before presented little problem, and all of the shape parameters and related functions remained the same. The additional term altered the working equation (31a) only, such that now

$$\frac{dZ}{dx} = \left| F(K) + \left[4 + f_1(K) \right] \frac{Z}{U_e} \frac{\partial U_e}{\partial t} \right.$$

$$+ \left[4 + 2f_1(K) - 2f_3(K) \right] \frac{Z R \dot{\alpha} \sin \phi}{U_e} \frac{\partial U_e}{\partial x}$$

$$\left. + 2 \left(\frac{C}{\delta}\right) Z f_3(K) R \dot{\alpha} \cos \phi \right| \frac{1}{U_e} \qquad (34)$$

Two problems now become apparent. First, some value must be assigned to the constant C. Secondly, the appearance of $\frac{1}{\delta}$ in the new term is undesirable, and renders Eq (34) unusable in its present form.

Consider the fact that, by injecting mass into the top of the boundary layer, a stagnation flow problem is being imposed upon the boundary layer. The impinging velocity of a two-dimensional potential flow near the stagnation point is given as

$$\frac{v}{V_\infty} = - ay \qquad \text{(Ref 7:96)}$$

Applied to the problem at hand, this would mean that at the outer edge of the boundary layer the velocity desired is:

$$V_e = - a\delta \, (R \dot{\alpha} \cos \phi)$$

The constant a is dependent upon the dimensions of the problem. In Appendix E it is argued that, for the Joukowski airfoil problem, a reasonable guess for the value of a is four. Using this,

$$C = 4\delta \tag{35}$$

and Eq (34) becomes

$$\frac{dZ}{dx} = \left| F(K) + \left[4 + f_1(K) \right] \frac{Z}{U_e} \frac{\partial U_e}{\partial t} \right.$$

$$+ \left[4 + 2f_1(K) - 2f_3(K) \right] \frac{Z \, R \, \dot{\alpha} \sin \phi}{U_e} \frac{\partial U_e}{\partial x}$$

$$\left. + 8 \, Z \, f_3(K) \, R \, \dot{\alpha} \cos \phi \right| \frac{1}{U_e} \tag{36}$$

Using Eqs (31b) and (36) as the working equations, solutions were again computed for various free-stream velocities and pitch rates. The results are shown in Figure 13, labeled "Mass Introduction (4δ)". The injection of this small amount of mass into the boundary layer has more than doubled the dynamic increase in stall angle of attack. This is attributed to the fact that the injected mass is accelerating, or imparting additional energy to, the fluid in the boundary layer, hence retarding separation.

The computer program used to calculate these solutions is included for reference in Appendix F.

The justification for the use of $a = 4$ in equation (35) that is outlined in Appendix E is somewhat arbitrary, and certainly arguments could be presented for other values of this constant. The possibility was considered that careful selection of this value might provide data that would match experimental data. In this interest, varicus values were tried. Figure 13 shows the results for $a = 20$, labeled "Mass Introduction (20δ)". It is apparent that the experimental results cannot be matched in this manner. It is interesting and possibly significant to note that, for the selected value $a = 4$, the slope of the plotted data becomes closely tangent to the slope of the experimental data.

This implies that still other factors, in addition to mass introduction, might be contributing to the dynamic stall effect, although it is clearly implied that mass introduction is an important contributor.

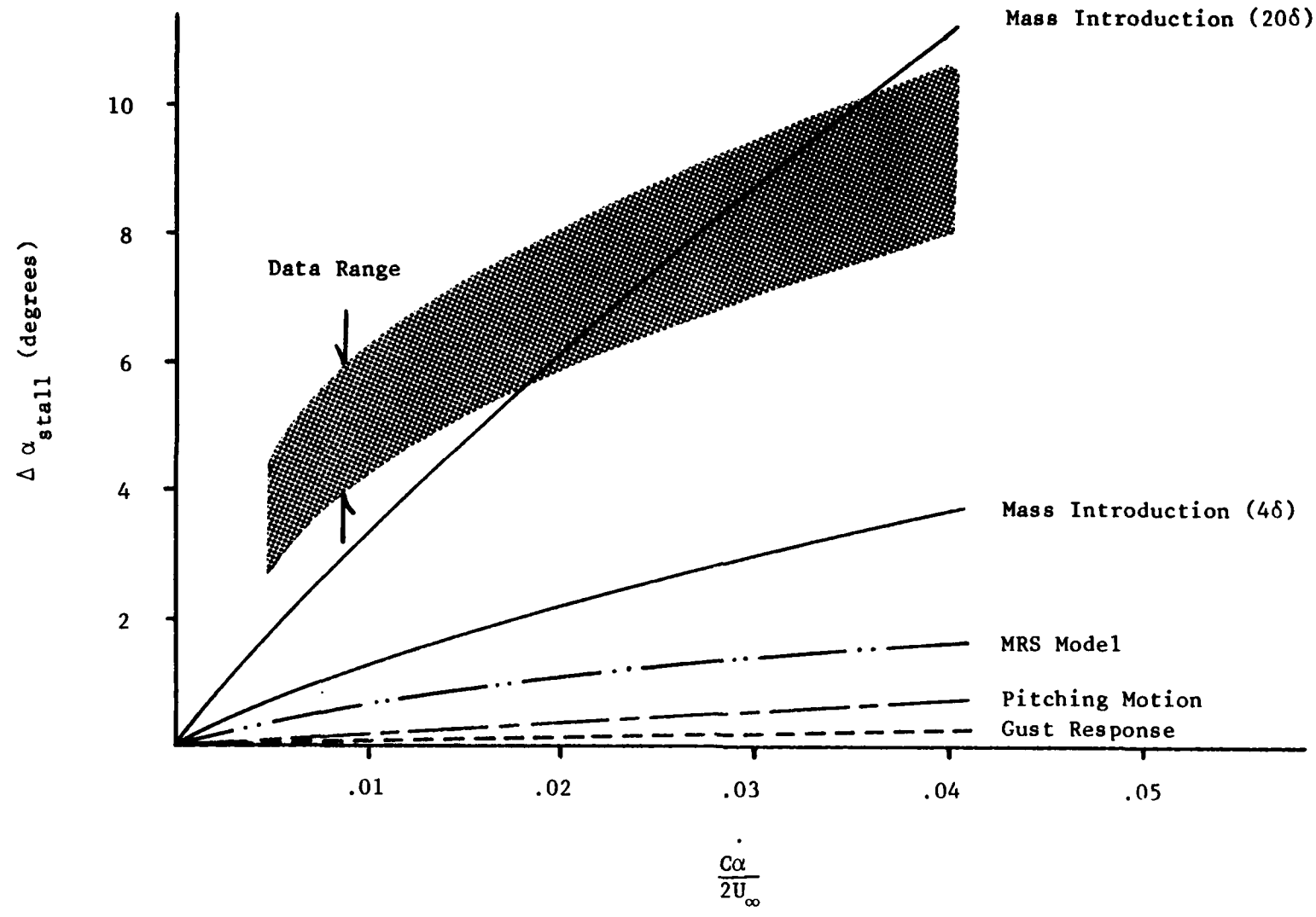

Figure 13. Effects Contributing to Change in Separation Angle of Attack Due to the Pitching Motion of an Airfoil

VI. Conclusions and Recommendations

Conclusions

For the case of an airfoil encountering a gust of constant $\dot{\alpha}$, the increase in dynamic stall angle of attack can be attributed almost exclusively to a reduction in the adversity of the pressure gradient on the upper surface of the airfoil.

The use of

$$\frac{\partial \delta_1}{\partial t} = -\frac{\delta}{2U_e}\frac{\partial U_e}{\partial t}$$

is acceptable for use as an equation of closure for the unsteady von Karman-Pohlhausen integral method. A conservative estimate of the error inflicted by its use causes an under-prediction of increase in dynamic stall angle of attack by less than 10%, and the analysis seems to indicate that the approximation is really much better than this estimate.

The increase in dynamic stall angle of attack for gust response is inversely proportional to, and a strong function of, the maximum thickness of the airfoil. It is inversely proportional to, and a weak function of, the maximum camber of the airfoil.

Contributing factors to the increase in dynamic stall angle of attack for an airfoil pitching at constant $\dot{\alpha}$ in a steady flow are:

a. A reduction in the adversity of the pressure gradient on the upper surface of the airfoil.

b. An effectively reduced free-stream velocity due to the downstream motion of the surface of the airfoil, causing further relaxation of the severity of the adverse pressure gradient.

c. A delay in boundary layer separation due to the fact that the motion of the airfoil surface allows the velocity gradient to build past the condition of zero wall shear to the condition of zero velocity and shear at some point in the boundary layer.

d. An acceleration of the fluid in the boundary layer due to mass introduction into the top of the boundary layer.

The factors above may not be all of the contributing effects, indicating that other phenomena should be considered to account for the total dynamic effect. However, it is clear that the mass introduction is an important contributor to the effect.

Recommendations

In considering the idea of mass introduction into the boundary layer of a pitching airfoil, the selection of 4δ as the appropriate constant was a rough estimate at best, and intended only to show trend on the solution. An in-depth study of the concept of mass introduction is appropriate.

In this report, the effect of the shedding of starting vortices due to the change in the airflow pattern about the airfoil has been assumed to have negligible contribution to the solution. Work currently in progress by K. Tupper in this area would indicate that this effect should be considered (Ref 14). A study combining the work of this report with that of Tupper seems a good step toward identifying other possible dynamic stall contributors.

Because of the success in incorporating constant $\dot{\alpha}$ (non-Newtonian) motion to the airfoil, there appears to be no fundamental reason why the method could not be extended to other motions, such as constant $\ddot{\alpha}$ (varying pitch rate).

Bibliography

1. McCroskey, W.J. "Unsteady Airfoils," Annual Review of Fluid Mechanics, 14: 285-311 (1982).

2. Kramer, Von Max "The Increase in $C_{L_{max}}$ of Airfoils with a Sudden Increase of Angle of Attack Gust Effect," English translation, Zeitschrift für Flugtechnik and Motorluftschiffahrt, 7: 185-189 (14 April 1932).

3. Docken, R.G. Jr., E.J. Jumper, and J.E. Hitchcock. "Theoretical Gust Response Prediction of a Joukowski Airfoil," Proceedings of the AIAA (Dayton-Cincinnati Section) 9th Annual Mini-Symposium on Aerospace Science and Technology. Wright-Patterson AFB, OH, March 1983.

4. Deekens, Arthur C. and William R. Keubler Jr. "A Smoke Tunnel Investigation of Dynamic Separation," Air Force Academy Aeronautics Digest - Fall 1978: 2-16 (February 1979).

5. Daley, Major Daniel C. Experimental Investigation of Dynamic Stall. MS Thesis, AFIT/GAE/AA/82D-6. School of Engineering, Air Force Institute of Technology, Wright-Patterson AFB, OH, 1983.

6. Docken, Capt. Richard G. Jr. Gust Response Prediction of an Airfoil Using a Modified Von Karman-Pohlhausen Technique. MS Thesis, AFIT/GAE/AA/82D-9. School of Engineering, Air Force Institute of Technology, Wright-Patterson AFB, OH, 1982.

7. Schlichting, Hermann. Boundary-Layer Theory (Seventh Edition). New York: McGraw-Hill Book Company, Inc., 1979.

8. Kuethe, Arnold M. and Chuen-Yen Chow. Foundations of Aerodynamics: Bases of Aerodynamic Design (Third Edition). New York: John Wiley and Sons, Inc., 1976.

9. Abbott, Ira H. and Albert E. Von Doenhoff. Theory of Wing Sections. New York: Dover Publications, Inc., 1959.

10. Shames, Irving H. Mechanics of Fluids. New York: McGraw-Hill Book Company, Inc., 1962.

11. Williams, James C. III. "Incompressible Boundary-Layer Separation," Annual Review of Fluid Mechanics, 9: 113-144 (1977).

12. Gadd, G.E., et al. "Approximate Methods of Solution," Laminar Boundary Layers, edited by L. Rosenhead. Oxford: Oxford University Press, 1963.

13. Smith, Charles E. Applied Mechanics: Dynamics (Second Edition). New York: John Wiley and Sons, Inc., 1982.

14. Tupper, Capt. K. W. The Effect of Trailing Vortices on the Production of Lift on an Airfoil Undergoing a Constant Rate of Change of Angle of Attack. MS Thesis, AFIT/GAE/AA/83D-26. School of Engineering, Air Force Institute of Technology, Wright-Patterson AFB, OH, 1983.

15. Kays, W. M. and M. E. Crawford. Convective Heat and Mass Transfer (Second Edition). New York: McGraw-Hill Book Company, Inc., 1980.

16. McCroskey, W. J. "Recent Developments in Dynamic Stall," Proceedings of a Symposium on Unsteady Aerodynamics. 1-33. University of Arizona, March 1975.

17. Hegna, Harwood A. "Numerical Prediction of Dynamic Forces on Arbitrarily Pitched Airfoils," AIAA Journal, 21: 161-162 (February 1983).

18. Ericsson, Lars E. and J. Peter Reding. "Unsteady Airfoil Stall, Review and Extension," Journal of Aircraft, 8: 609-616 (August 1971).

19. Carr, Lawrence W., et al. Analysis of the Development of Dynamic Stall Based on Oscillating Airfoil Experiments. NASA TN D-8382. Washington: National Aeronautics and Space Administration, January 1977.

20. Ericsson, Lars E. and J. Peter Reding. "Dynamic Stall Analysis in Light of Recent Numerical and Experimental Results," Journal of Aircraft, 13: 248-255 (April 1976).

21. Ghia, U. Class Notes for AE5.20, "Viscous Flow Theory," School of Engineering, Air Force Institute of Technology, 1982.

22. Smith, M. Class Notes for AE6.36, "Wing and Airfoil Theory," School of Engineering, Air Force Institute of Technology, 1983.

23. Ericsson, Lars E. and J. Peter Reding. Analytical Prediction of Dynamic Stall Characteristics. AIAA Paper No. 72-682. New York: American Institute of Aeronautics and Astronautics, June 1972.

24. Jumper, E. J. and J. E. Hitchcock. "Theoretical Investigation of Dynamic Stall Using a Momentum-Integral Method," Proceedings of the Workshop on Unsteady Separated Flow. United States Air Force Academy CO, August 1983.

Appendix A: Derivation of the Unsteady Momentum-Integral Equation

The momentum-integral equation for unsteady flow is derived by integrating the equation of motion over the thickness of the boundary layer. The equation of motion in turn is derived by applying the principles of continuity and conservation of momentum in the direction of flow to an incremental control volume in the boundary layer.

The principle of continuity (mass conservation) states that the net rate of mass flow across the control surface must equal the time rate of mass reduction within the control volume. Referring to Figure 14, it is shown that

$$\dot{m}_{top} + \left[\int_0^h \rho u dy + \frac{\partial}{\partial x} \int_0^h \rho u dy dx \right] - \int_0^h \rho u dy$$

$$= - \frac{\partial}{\partial t} \int_0^h \rho dy$$

For incompressible flow, i.e. ρ = constant, the last term in this expression is zero. Therefore

$$\dot{m}_{top} = - \frac{\partial}{\partial x} \int_0^h \rho u dy dx \qquad (A1)$$

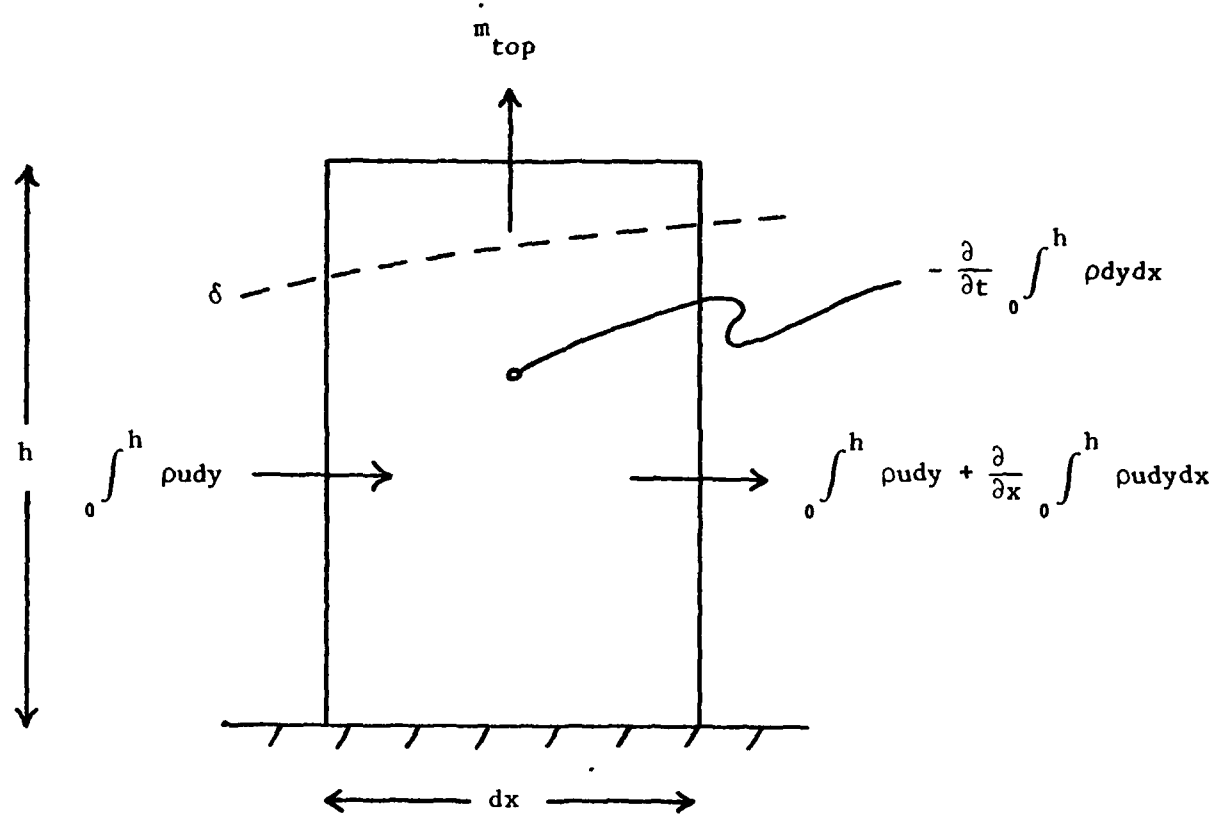

Figure 14. Mass Conservation in a Boundary Layer Control Volume

The principle of momentum conservation (in the x-direction) requires that the sum of the forces acting on the fluid in the control volume is equal to the net rate of transport of momentum across the control surface plus the time flux of momentum within the control volume. Referring to Figure 15, it is shown that

$$-\tau_w dx + \int_0^h P dy - \left[\int_0^h P dy + \frac{\partial}{\partial x} \int_0^h P dy dx \right] = U_e \dot{m}_{top}$$

$$+ \left[\int_0^h \rho u u dy + \frac{\partial}{\partial x} \int_0^h \rho u u dy dx \right] - \int_0^h \rho u u dy + \frac{\partial}{\partial t} \int_0^h \rho u dy dx$$

Simplifying and rearranging terms,

$$\frac{\partial}{\partial x} \int_0^h \rho u u dy dx + U_e \dot{m}_{top} + \frac{\partial}{\partial t} \int_0^h \rho u dy dx$$

$$= -\tau_w dx - \frac{\partial}{\partial x} \int_0^h P dy dx \qquad \text{(A2)}$$

Substituting Eq (A1) for the unknown term in (A2),

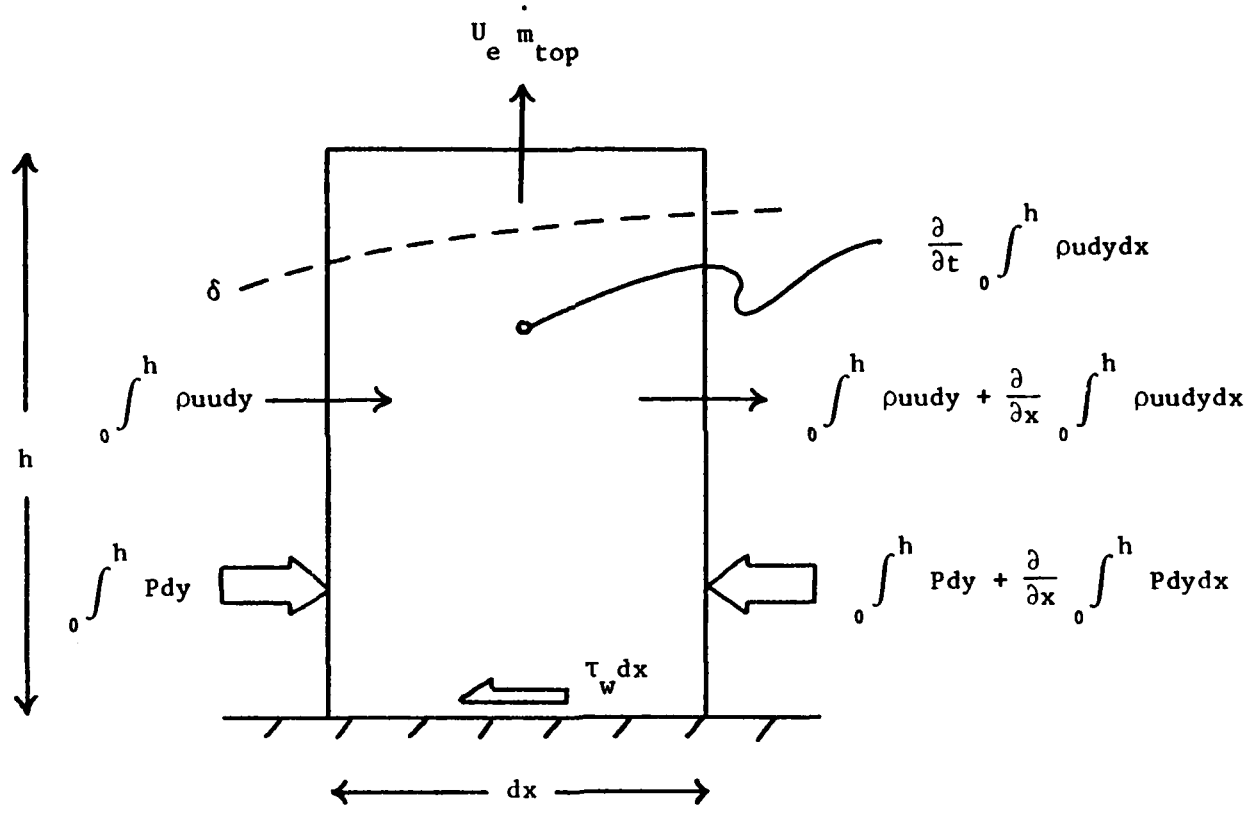

Figure 15. Momentum Conservation in a Boundary Layer Control Volume

$$\frac{\partial}{\partial x}\int_0^h \rho u u dy dx - U_e \frac{\partial}{\partial x}\int_0^h \rho u dy dx + \frac{\partial}{\partial t}\int_0^h \rho u dy dx$$

$$= -\tau_w dx - \frac{\partial}{\partial x}\int_0^h P dy dx \qquad (A3)$$

Note that, since the integrals are taken in the y-direction, the partial derivatives with respect to dimension x (and also time) can be arbitrarily brought inside the integrals. In addition, by boundary layer assumptions, the pressure gradient in the x-direction is assumed to be the total (spatial) pressure gradient. Employing these concepts, and dividing the entire equation by ρdx, Eq (A3) becomes

$$\int_0^h \frac{\partial}{\partial x}(uu) dy - U_e \int_0^h \frac{\partial u}{\partial x} dy + \frac{\partial}{\partial t}\int_0^h u dy$$

$$= -\frac{\tau_w}{\rho} - \frac{1}{\rho}\int_0^h \frac{dP}{dx} dy \qquad (A4)$$

The Euler's equation of motion for unsteady flow can be shown to be

$$-\frac{1}{\rho}\frac{dP}{dx} = U_e \frac{\partial U_e}{\partial x} + \frac{\partial U_e}{\partial t} \qquad \text{(Ref 27)}$$

This may be applied to Eq (A4) in substitution for the pressure gradient. After rearranging terms, Eq (A4) now becomes

$$- \int_0^h \frac{\partial}{\partial x}(uu)dy + U_e \int_0^h \frac{\partial u}{\partial x} dy + \int_0^h U_e \frac{\partial U_e}{\partial x} dy$$

$$- \frac{\partial}{\partial t} \int_0^h u dy + \int_0^h \frac{\partial U_e}{\partial t} dy = \frac{\tau_w}{\rho} \qquad \text{(A5)}$$

Consider the time variant terms of Eq (A5):

$$- \frac{\partial}{\partial t} \int_0^h u dy + \int_0^h \frac{\partial U_e}{\partial t} dy = \frac{\partial}{\partial t} \int_0^h (U_e - u)dy$$

Further, since U_e is independent of y,

$$- \frac{\partial}{\partial t} \int_0^h u dy + \int_0^h \frac{\partial U_e}{\partial t} dy = \frac{\partial}{\partial t} U_e \int_0^h (1 - \frac{u}{U_e})dy \qquad \text{(A6)}$$

Now consider the spatially variant terms of Eq (A5):

$$- \int_0^h \frac{\partial}{\partial x}(uu)dy + U_e \int_0^h \frac{\partial u}{\partial x} dy + \int_0^h U_e \frac{\partial U_e}{\partial x} dy$$

$$= - \int_0^h \frac{\partial}{\partial x}(uu)dy + \left[\int_0^h \frac{\partial}{\partial x}(uU_e)dy - \int_0^h u \frac{\partial U_e}{\partial x} dy \right]$$

$$+ \int_0^h U_e \frac{\partial U_e}{\partial x} dy$$

Simplifying,

$$- \int_0^h \frac{\partial}{\partial x}(uu)dy + U_e \int_0^h \frac{\partial u}{\partial x} dy + \int_0^h U_e \frac{\partial U_e}{\partial x} dy$$

$$= \int_0^h \frac{\partial}{\partial x}(uU_e - uu)dy + \int_0^h \frac{\partial U_e}{\partial x}(U_e - u)dy$$

And since U_e and $\frac{\partial U_e}{\partial x}$ are independent of y,

$$- \int_0^h \frac{\partial}{\partial x}(uu)dy + U_e \int_0^h \frac{\partial u}{\partial x} dy + \int_0^h U_e \frac{\partial U_e}{\partial x} dy$$

$$= \frac{\partial}{\partial x} U_e^2 \int_0^h \frac{u}{U_e}(1 - \frac{u}{U_e})dy + U_e \frac{\partial U_e}{\partial x} \int_0^h (1 - \frac{u}{U_e})dy \qquad (A7)$$

Substitution of Eqs (A6) and (A7) into Eq (A5) yields the momentum-integral equation for unsteady flow:

$$\frac{\partial}{\partial x} U_e^2 \int_0^h \frac{u}{U_e}\left(1 - \frac{u}{U_e}\right)dy + U_e \frac{\partial U_e}{\partial x} \int_0^h \left(1 - \frac{u}{U_e}\right)dy$$

$$+ \frac{\partial}{\partial t} U_e \int_0^h \left(1 - \frac{u}{U_e}\right)dy = \frac{\tau_w}{\rho} \qquad \text{(A8)}$$

Appendix B: Development of the von Karman-Pohlhausen Method for Unsteady Flow

By comparing the unsteady momentum-integral equation (A8) with the definitions of the boundary layer displacement and momentum thickness in their integral form (Ref 7:140-141), it is evident that, for arbitrary h,

$$\frac{\partial}{\partial x}\left(U_e^{\,2}\,\delta_2\right) + U_e\,\frac{\partial U_e}{\partial x}\,\delta_1 + \frac{\partial}{\partial t}\left(U_e\,\delta_1\right) = \frac{\tau_w}{\rho}$$

Expanding the first and third terms and rearranging yields

$$\left(2\delta_2 + \delta_1\right) U_e\,\frac{\partial U_e}{\partial x} + U_e^{\,2}\,\frac{\partial \delta_2}{\partial x} + U_e\,\frac{\partial \delta_1}{\partial t} + \delta_1\,\frac{\partial U_e}{\partial t} = \frac{\tau_w}{\rho}$$

At this point an equation of closure, Eq (5), is used to substitute for the difficult term $\frac{\partial \delta_1}{\partial t}$. This closure equation and its validity is discussed at length in Section III. The result is

$$\left(2\delta_2 + \delta_1\right) U_e\,\frac{\partial U_e}{\partial x} + U_e^{\,2}\,\frac{\partial \delta_2}{\partial x} + \frac{1}{2}\,\delta_1\,\frac{\partial U_e}{\partial t} = \frac{\tau_w}{\rho}$$

Multiplying this equation by $\frac{\delta_2}{\nu U_e}$ yields

$$(2 + \frac{\delta_1}{\delta_2}) \frac{\delta_2^2}{\nu} \frac{\partial U_e}{\partial x} + U_e \frac{\delta_2}{\nu} \frac{\partial \delta_2}{\partial x} + \frac{1}{2U_e} \frac{\delta_1}{\delta_2} \frac{\delta_2^2}{\nu} \frac{\partial U_e}{\partial t} = \frac{\tau_w \delta_2}{\mu U_e}$$

Finally, by adding and subtracting the quantity

$$(2 + \frac{1}{2} \frac{\delta_1}{\delta_2}) \frac{\delta_2^2}{\nu} (\frac{1}{U_e} \frac{\partial U_e}{\partial t})$$

the momentum-integral equation becomes

$$(2 + \frac{\delta_1}{\delta_2}) \frac{\delta_2^2}{\nu} (\frac{\partial U_e}{\partial x} + \frac{1}{U_e} \frac{\partial U_e}{\partial t}) + U_e \frac{\delta_2}{\nu} \frac{\partial \delta_2}{\partial x}$$

$$- (2 + \frac{1}{2} \frac{\delta_1}{\delta_2}) \frac{\delta_2^2}{\nu} (\frac{1}{U_e} \frac{\partial U_e}{\partial t}) = \frac{\tau_w \delta_2}{\mu U_e} \qquad \text{(B1)}$$

The velocity profile of the boundary layer must satisfy the following boundary conditions:

at $y = 0$, $u = 0$ (B2a)

$$\nu \frac{\partial^2 u}{\partial y^2} = -\left(U_e \frac{\partial U_e}{\partial x} + \frac{\partial U_e}{\partial t}\right) \quad \text{(B2b)}$$

at $y = \delta$, $u = U_e$ (B2c)

$$\frac{\partial u}{\partial y} = 0 \quad \text{(B2d)}$$

$$\frac{\partial^2 u}{\partial y^2} = 0 \quad \text{(B2e)}$$

Since the existence of five boundary conditions will allow for the solution of five free constants, the velocity profile may be expressed as a fourth-degree polynomial, where $\eta = \frac{y}{\delta}$:

$$\frac{u}{U_e} = A + B\eta + C\eta^2 + D\eta^3 + E\eta^4 \quad \text{(B3)}$$

Applying (B2a) yields

$$A = 0 \quad \text{(B4a)}$$

Applying (B2c) yields

$$1 = B + C + D + E \quad \text{(B4b)}$$

Applying (B2d) yields

$$0 = B + 2C + 3D + 4E \tag{B4c}$$

Applying (B2e) yields

$$0 = 2C + 6D + 12E \tag{B4d}$$

Finally, (B2b) is applied such that

$$\frac{U_e}{\delta^2} \frac{\partial^2(u/U_e)}{\partial(y/\delta)^2} = 2C + 6D\eta + 12E\eta^2$$

which, evaluating at $\eta = 0$, yields

$$2C = -\frac{\delta^2}{\nu} \left(\frac{\partial U_e}{\partial x} + \frac{1}{U_e} \frac{\partial U_e}{\partial t}\right) \tag{B4e}$$

The dimensionless shape parameter is now defined as

$$\Lambda = \frac{\delta^2}{\nu} \left(\frac{\partial U_e}{\partial x} + \frac{1}{U_e} \frac{\partial U_e}{\partial t}\right) \tag{B5}$$

If Eq (B5) is substituted into (B4e), the set of equations (B4a-e) can be solved simultaneously in terms of Λ:

$$A = 0$$

$$B = 2 + \frac{\Lambda}{6}$$

$$C = -\frac{\Lambda}{2}$$

$$D = -2 + \frac{\Lambda}{2}$$

$$E = 1 - \frac{\Lambda}{6}$$

The velocity profile, Eq (B3), thus becomes

$$\frac{u}{U_e} = (2\eta - 2\eta^3 + \eta^4) + \frac{\Lambda}{6}(\eta - 3\eta^2 + 3\eta^3 - \eta^4) \qquad \text{(B6)}$$

Recall that the displacement and momentum thickness are defined as

$$\frac{\delta_1}{\delta} = \frac{1}{\delta}\int_0^h (1 - \frac{u}{U_e})dy$$

and

$$\frac{\delta_2}{\delta} = \frac{1}{\delta}\int_0^h \frac{u}{U_e}\left(1 - \frac{u}{U_e}\right)dy$$

Since $u = U_e$ for $h \geq \delta$, integration beyond $h = \delta$ yields nothing, and the above equations may be written

$$\frac{\delta_1}{\delta} = \int_0^1 \left(1 - \frac{u}{U_e}\right)d\eta$$

and

$$\frac{\delta_2}{\delta} = \int_0^1 \frac{u}{U_e}\left(1 - \frac{u}{U_e}\right)d\eta$$

Using Eq (B6), the above integrations can now be performed, yielding

$$\frac{\delta_1}{\delta} = \frac{3}{10} - \frac{\Lambda}{120} \qquad \text{(B7)}$$

and

$$\frac{\delta_2}{\delta} = \frac{37}{315} - \frac{\Lambda}{945} - \frac{\Lambda^2}{9072} \qquad \text{(B8)}$$

The shear stress at the wall is defined as

$$\tau_w = \mu \frac{\partial u}{\partial y} \qquad \text{at} \quad y = 0$$

Therefore, by using Eq (B6) and evaluating at $\eta = 0$,

$$\frac{\tau_w \delta}{\mu U_e} = 2 + \frac{\Lambda}{6} \tag{B9}$$

From this, the separation criteria, defined as the point at which the shear stress at the wall becomes zero, can be seen to be

$$\Lambda = -12 \tag{B10}$$

The last form of the momentum-integral equation, (B1), encourages additional parameters to be defined as:

$$Z = \frac{\delta_2^2}{\nu} \tag{B11}$$

$$K = Z\left(\frac{\partial U_e}{\partial x} + \frac{1}{U_e}\frac{\partial U_e}{\partial t}\right) = \Lambda\left(\frac{37}{315} - \frac{\Lambda}{945} - \frac{\Lambda^2}{9072}\right)^2 \tag{B12}$$

$$f_1(K) = \frac{\delta_1}{\delta_2} = \left(\frac{3}{10} - \frac{\Lambda}{120}\right)\left(\frac{37}{315} - \frac{\Lambda}{945} - \frac{\Lambda^2}{9072}\right)^{-1} \tag{B13}$$

and

$$f_2(K) = \frac{\tau_w \delta_2}{\mu U_e} = \left(2 + \frac{\Lambda}{6}\right)\left(\frac{37}{315} - \frac{\Lambda}{945} - \frac{\Lambda^2}{9072}\right) \tag{B14}$$

Note that using Eq (B11),

$$U_e \frac{\delta_2}{\nu}\frac{\partial \delta_2}{\partial x} = \frac{1}{2}\frac{U_e}{\nu}\frac{\partial(\delta_2^2)}{\partial x} = \frac{1}{2} U_e \frac{dZ}{dx} \tag{B15}$$

Now, the relationships in Eqs (B11-15) are substituted into the momentum-integral equation (B1) to yield

$$\left[2 + f_1(K)\right]K + \frac{U_e}{2}\frac{dZ}{dx} - \left[2 + \frac{1}{2} f_1(K)\right]\frac{Z}{U_e}\frac{\partial U_e}{\partial t} = f_2(K)$$

Rearranging of terms yields

$$U_e \frac{dZ}{dx} - \left[4 + f_1(K)\right] \frac{Z}{U_e} \frac{\partial U_e}{\partial t} = 2 f_2(K) - 4K - 2 K f_1(K) \qquad \text{(B16)}$$

One final parameter is defined as

$$F(K) = 2 f_2(K) - 4K - 2 K f_1(K) \qquad \text{(B17)}$$

By substituting Eq (B17) into (B16) and then solving for $\frac{dZ}{dx}$,

$$\frac{dZ}{dx} = \left| F(K) + \left[4 + f_1(K)\right] \frac{Z}{U_e} \frac{\partial U_e}{\partial t} \right| \frac{1}{U_e} \qquad \text{(B18)}$$

and solving Eq (B12) for Z yields

$$Z = K \left(\frac{\partial U_e}{\partial x} + \frac{1}{U_e} \frac{\partial U_e}{\partial t}\right)^{-1} \qquad \text{(B19)}$$

Eqs (B18) and (B19) are the "working" equations, which are the modified equations that can be used to solve an unsteady boundary layer flow using the von Karman-Pohlhausen method.

Appendix C: Method of Solution

By selection of appropriate dimensions and position, a circle in one frame of reference can be transformed into a Joukowski airfoil of desired thickness and camber in another frame of reference by means of a complex function, commonly known as a Joukowski transformation (Ref 9:50-53). Further, a velocity on the surface of a circular cylinder can be likewise transformed to a velocity on the surface of the airfoil, such that for any given point on the airfoil at any given angle of attack a potential flow velocity is obtainable (Ref 9:53-60). By standard difference methods, then, the required partial derivatives of the potential velocity can also be obtained. This method of determining geometry, velocities, and partial derivatives, is described in depth in Reference 6, and will not be repeated here; however, the application of this method can be observed in Appendix F.

In using the von Karman-Pohlhausen technique calculation begins at the stagnation point. At this point it is known that $U_e = 0$ and $\frac{\partial U_e}{\partial x}$ is finite and not equal to zero. This poses problems with the calculation of $\frac{dZ}{dx}$. First, the solution will be initiated as a steady flow problem, with the pitching motion only considered after a finite number of small incremental steps, with negligible effect on accuracy of the final solution. Now it can be shown that F(K) must vanish simultaneously with U_e at the stagnation point to avoid an infinite value of $\frac{dZ}{dx}$. Solution of Eq (B17) for F(K) = 0 yields the following initial values:

$$\Lambda_0 = 7.052$$

$$K_0 = 0.0770$$

Now $\frac{dZ}{dx}$ is of indeterminate form $\frac{0}{0}$, which can be evaluated by a limiting process (Ref 7:211). The result is

$$Z_0 = K_0 \left(\frac{\partial U_e}{\partial x}\right)_0^{-1} = 0.0770 \left(\frac{\partial U_e}{\partial x}\right)_0^{-1}$$

and

$$\left(\frac{dZ}{dx}\right)_0 = -0.0652 \left(\frac{\partial^2 U_e}{\partial x^2}\right)_0 \left(\frac{\partial U_e}{\partial x}\right)_0^{-2}$$

With these initial values, the solution can now be "marched" forward along the airfoil as follows:

a. Compute Z, in the manner of

$$Z_1 = Z_0 + \left(\frac{dZ}{dx}\right)_0 dx$$

where dx is an increment of arc length along the airfoil.

b. Compute a new value of K from Eq (B19).

c. Compute a new value of Λ from this K, either by solution of Eq (B12) or by a curve-fit routine.

d. Compute a new value of F(K) and $f_1(K)$ by solution of Eqs (B13), (B14), and (B17). For the steady flow solution, F(K) may be approximated by the linear relationship

$$F(K) = .47 - 6K \quad \text{(Ref 7:213-214)}$$

with reasonable accuracy.

e. Compute a new value of $\frac{dZ}{dx}$ using Eq (B18).

f. Now, with new values for both Z and $\frac{dZ}{dx}$, this procedure can be looped back to step a, continuing with a new incremental step.

The value of Λ (or K) can be examined at any point and compared with the known separation value

$$\Lambda = -12$$

or

$$K = -.1567$$

For a given free-stream velocity and pitch rate, this procedure was used, iterating between different initial angles of attack, until separation was indicated at quarter-chord, and the final angle of attack recorded.

Appendix D: Derivation of the Hypothetical Body Forces

The conservation of momentum relationship is developed by applying Newton's law in the form

$$\bar{F} = \frac{D}{Dt}(m\bar{V}) = m\bar{a}$$

This analysis is only valid if accelerations are measured in an inertial reference frame. In order to develop a momentum conservation relationship for a non-inertial control volume, as is the case in the boundary layer of a pitching airfoil, it is first necessary to analyze the inertial acceleration of a particle in the control volume (Ref 10:109-114).

Consider the problem as shown in Figure 16. Here the reference frames are to be interpreted as

F - frame = fixed in inertial space

f - frame = fixed in the geometry of the airfoil

xyz - frame = fixed in the control volume

By the geometry shown in Figure 16, the coordinate transformations are

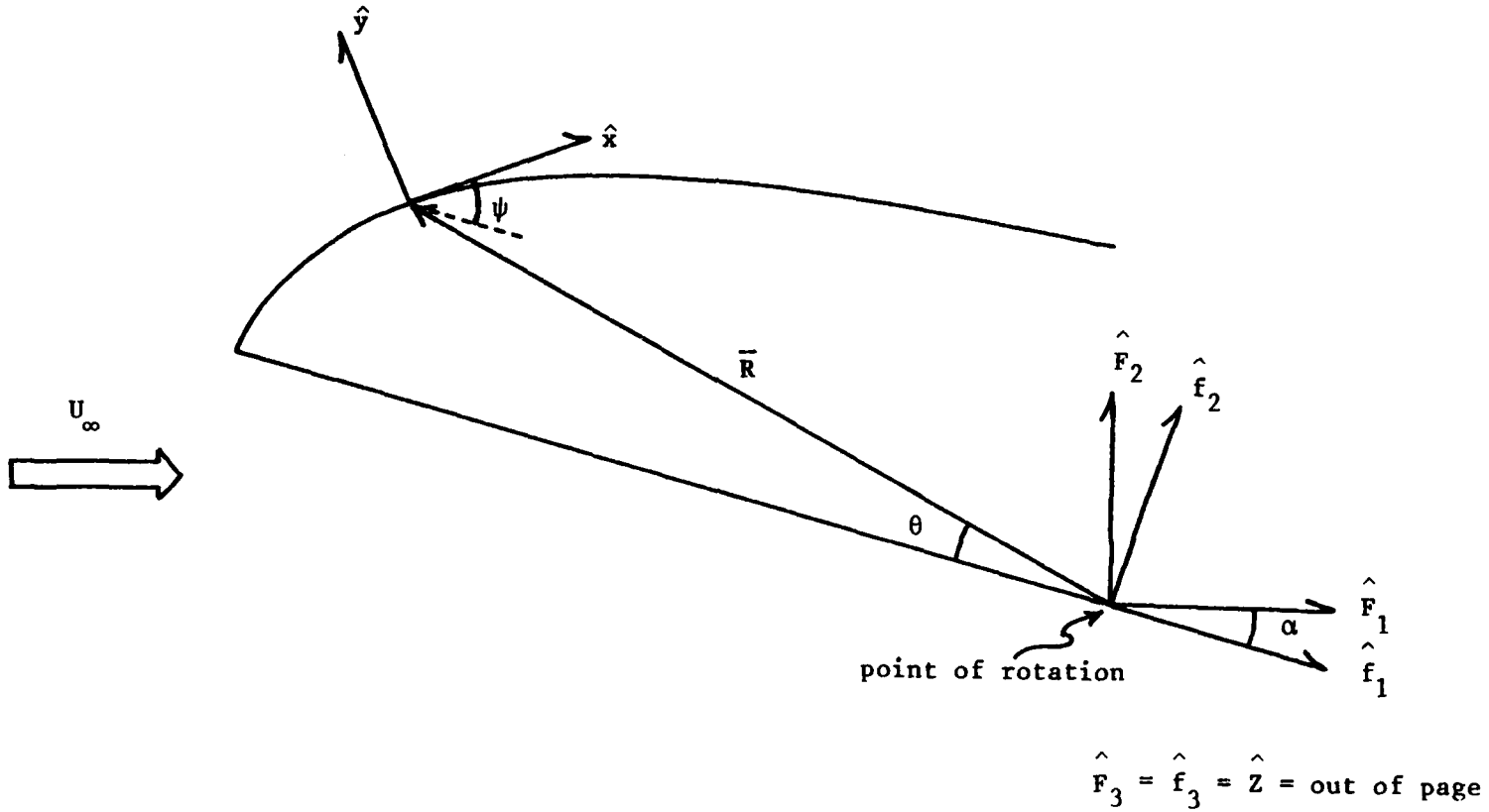

Figure 16. Reference Frame Analysis of Pitching Airfoil Problem

$$\hat{F}_1 = (\cos \alpha)\hat{f}_1 + (\sin \alpha)\hat{f}_2$$

$$\hat{F}_2 = (-\sin \alpha)\hat{f}_1 + (\cos \alpha)\hat{f}_2 \qquad \text{(D1)}$$

$$\hat{F}_3 = \hat{f}_3$$

and

$$\hat{f}_1 = (\cos \psi)\hat{x} + (-\sin \psi)\hat{y}$$

$$\hat{f}_2 = (\sin \psi)\hat{x} + (\cos \psi)\hat{y} \qquad \text{(D2)}$$

$$\hat{f}_3 = \hat{Z}$$

Combining relationships in Eqs (D1) and (D2) yields

$$\hat{F}_1 = \cos (\alpha-\psi)\ \hat{x} + \sin (\sin (\alpha-\psi)\ \hat{y}$$

$$\hat{F}_2 = -\sin (\alpha-\psi)\ \hat{x} + \cos (\alpha-\psi)\ \hat{y} \qquad \text{(D3)}$$

$$\hat{F}_3 = \hat{Z}$$

It can also be seen that the angular velocity of the xyz - frame with respect to the F - frame is

$$\bar{\omega}_{xyz} = -\dot{\alpha}\,\hat{F}_3 = -\dot{\alpha}\,\hat{Z} \tag{D4}$$

Now, referring to Figure 17, consider the motion of a particle P. The position vector of the particle is

$$\bar{P} = \bar{R} + \bar{r}$$

The velocity of P with respect to the F - frame is

$$\left(\frac{d\bar{P}}{dt}\right)_F = \left(\frac{d\bar{R}}{dt}\right)_F + \left(\frac{d\bar{r}}{dt}\right)_F$$

Using the relationship of derivatives of a vector in a rotating reference frame (Ref 13:334-336),

$$\bar{V}_F = \dot{\bar{R}}_F + \left(\frac{d\bar{r}}{dt}\right)_x + \bar{\omega}_{xyz} \times \bar{r}$$

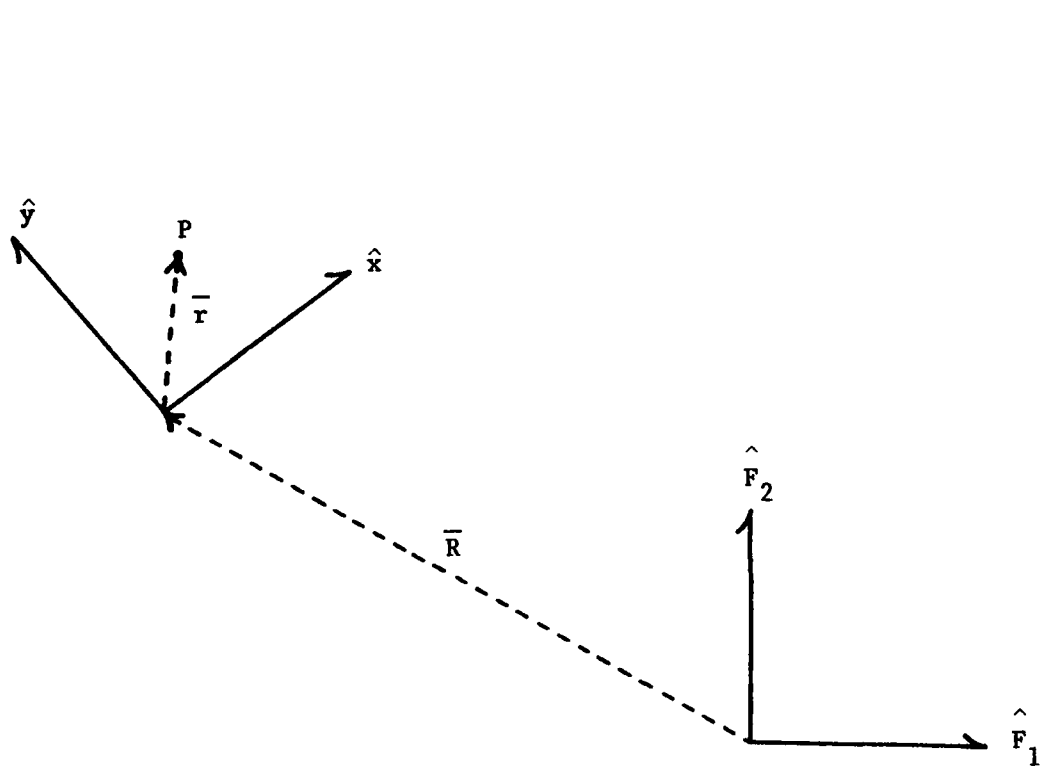

Figure 17. Motion of a Particle in a Translating and Rotating Reference Frame

Differentiating again to find the acceleration of P with respect to the F - frame gives

$$\frac{{}^{F}d}{dt}({}^{F}\bar{V}) = \frac{{}^{F}d}{dt}({}^{F}\dot{\bar{R}}) + \frac{{}^{F}d}{dt}({}^{x}\frac{d\bar{r}}{dt}) + \frac{{}^{F}d\bar{\omega}}{dt} \times \bar{r} + \bar{\omega} \times \frac{{}^{F}d\bar{r}}{dt}$$

This reduces to

$${}^{F}\bar{a} = {}^{F}\ddot{\bar{R}} + {}^{x}\bar{a} + 2\bar{\omega} \times {}^{x}\bar{V} + \dot{\bar{\omega}} \times \bar{r} + \bar{\omega} \times (\bar{\omega} \times \bar{r})$$

Newton's law can now be applied to the inertial acceleration:

$$dF = dm\left[{}^{F}\ddot{\bar{R}} + {}^{x}\bar{a} + 2\bar{\omega} \times {}^{x}\bar{V} + \dot{\bar{\omega}} \times \bar{r} + \bar{\omega} \times (\bar{\omega} \times \bar{r})\right]$$

Solving for acceleration in the xyz - frame,

$$dF - dm\left[{}^{F}\ddot{\bar{R}} + 2\bar{\omega} \times {}^{x}\bar{V} + \dot{\bar{\omega}} \times \bar{r} + \bar{\omega} \times (\bar{\omega} \times \bar{r})\right] = dm({}^{x}\bar{a}) \qquad (D5)$$

If the bracketed terms in Eq (D5) are thought of in terms of forces, in fact body forces since they are multiplied by mass, then this is essentially a valid representation of Newton's law for a non-inertial reference frame. Conservation of momentum in this frame can now be implied in the usual manner.

The hypothetical body force in question then is

$$d\bar{B} = - dm \left[\ddot{\bar{R}} + 2\bar{\omega} \times {}^{x}\bar{V} + \dot{\bar{\omega}} \times \bar{r} + \bar{\omega} \times (\bar{\omega} \times \bar{r}) \right] \qquad (D6)$$

Referring again to Figure 16, it can be seen that, for a given control volume on the surface of the airfoil, θ and ψ are constant, the magnitude of $\bar{R}$ is constant, and $\dot{\alpha}$ is considered constant for the situation under investigation. In light of these consideration, and given the relationships in Eqs (D3) and (D4), each of the bracketed terms in Eq (D6) can be evaluated in the xyz - frame:

$$\ddot{\bar{R}} = R \dot{\alpha}^2 \left[\cos(\theta+\psi)\hat{x} - \sin(\theta+\psi)\hat{y} \right]$$

$$2\bar{\omega} \times {}^{x}\bar{V} = 2 \dot{\alpha} (v\hat{x} - u\hat{y})$$

$$\dot{\bar{\omega}} \times \bar{r} = 0$$

$$\bar{\omega} \times (\bar{\omega} \times \bar{r}) = - \dot{\alpha}^2 (x\hat{x} + y\hat{y})$$

Letting $\phi = (\theta + \psi)$, the x-component of the hypothetical body force is

$$dB_x = - dm \left[R \dot{\alpha}^2 \cos \phi + 2 \dot{\alpha} v - \dot{\alpha}^2 x \right] \tag{D7}$$

which will be used in the analysis of momentum in the x-direction.

A physical explanation of the hypothetical body forces is as follows:

$\ddot{\underline{F}}_R$ represents the component of acceleration due to the translation motion of the control volume.

$2\bar{\omega} \times {}^{x}\bar{V}$ represents the coriolis component of acceleration due to the rotational motion of the control volume.

$\bar{\omega} \times (\bar{\omega} \times \bar{r})$ represents the centripetal component of acceleration due to the rotational motion of the control volume (Ref 13:350-353).

Appendix E: Estimation of Mass Introduction Constant

In the vicinity of the stagnation point, the frictionless potential flow velocity distribution is given by

$$\frac{u_s}{U_\infty} = as \tag{E1a}$$

and

$$\frac{u_r}{U_\infty} = -ar \qquad \text{(Ref 7:96)} \tag{E1b}$$

where a is a constant and the velocities and dimensions are as defined in Figure 18. While it is the radial velocity equation (E1b) that is to be used in the mass introduction solution, the constant a can be approximated by examination of the tangential velocity equation (E1a).

Consider the flow about a circular cylinder in a uniform stream, as depicted in Figure 18. The velocity at the surface of the cylinder can be shown to be

$$u_s = 2\,U_\infty \sin\theta \qquad \text{(Ref 8:90)} \tag{E2}$$

For the region near the stagnation point, θ is small, and the assumption is made that $\sin\theta \sim \theta$; thus

AD-A136 897 INVESTIGATION OF EFFECTS CONTRIBUTING TO DYNAMIC STALL USING A MOMENTUM-I.. (U) AIR FORCE INST OF TECH WRIGHT-PATTERSON AFB OH SCHOOL OF ENGI.. J S LAWRENCE

2/2

UNCLASSIFIED DEC 83 AFIT/GAE/AA/83D-12 F/G 20/4 NL

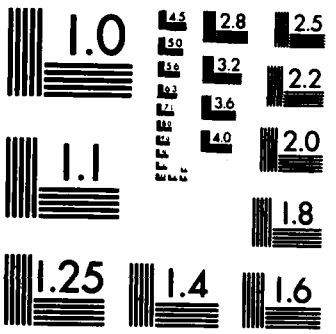

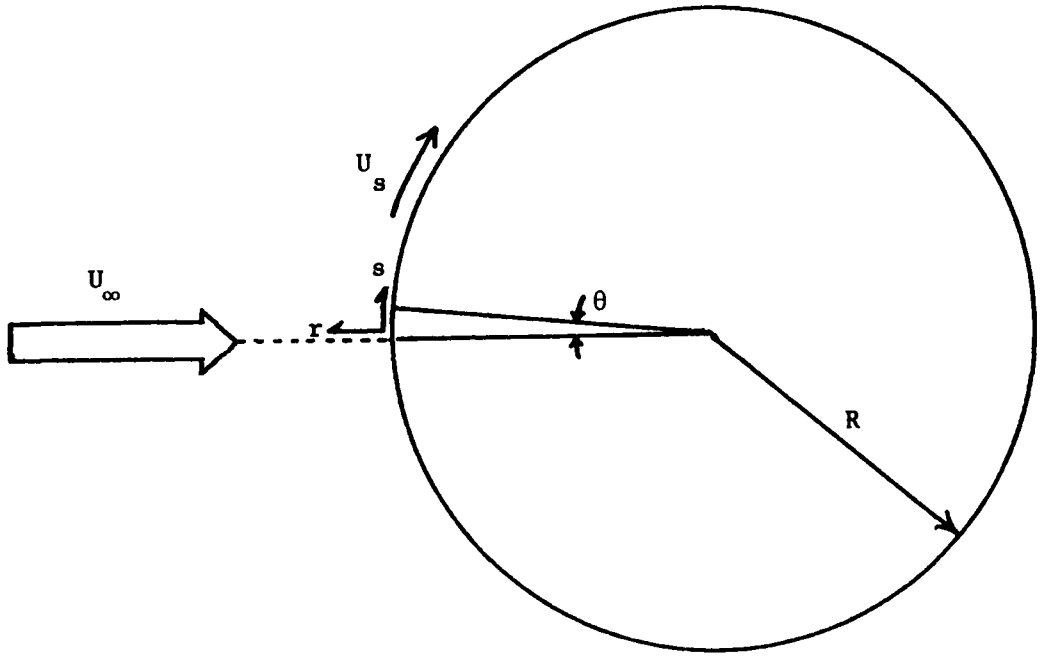

Figure 18. Flow About a Circular Cylinder in a Uniform Stream

$$u_s \simeq 2 U_\infty \theta \tag{E3}$$

The velocity gradient in the s-direction is

$$\frac{du_s}{ds} = \frac{1}{R} \frac{du_s}{d\theta} = \frac{2U_\infty}{R} \tag{E4}$$

By integrating Eq (E4) with respect to s, the velocity is obtained as a function of the surface coordinate:

$$u_s = \frac{2 U_\infty s}{R} \tag{E5}$$

Comparison of Eqs (E1a) and (E5) yields

$$a = \frac{2}{R} \tag{E6}$$

for the given circular cylinder.

The Joukowski airfoil of interest is obtained by transformation from a circular cylinder in a flow field as described in Eq (E2). The real-axis

radius of this cylinder transforms to the half-chord of the Joukowski airfoil. In the solution method, distances on the surface of the airfoil are non-dimensionalized with respect to the chord of the airfoil. Then letting $R = \frac{C}{2}$, Eq (E6) in non-dimensional form becomes

$$a = 4 \tag{E7}$$

Appendix F: Computer Program POHL6

```
*
*
*       LAWRENCE, JOHN S.
*       GAE-83D
*
*
*       This program is adapted from program "POHL2", Docken,
*       GAE-82D, and will be used to continue analysis work in the
*       area of dynamic stall effects.  The representative airfoil is
*       a 15% Joukowski, pitching at a constant rate about its mid-
*       chord in a steady freestream.  Mass is being injected from
*       the freestream into the boundary layer as a result of the
*       non-Newtonian motion of the airfoil. Symbology within the
*       program is as follows:
*         EI = imaginary unit; i.e., square root of -1.
*         RADIUS = radius of circular cylinder.
*         AMU = offset distance of center of circular cylinder.
*         ALPHA = angle of attack, in degrees.
*         ADOT1 = pitch rate, in degrees per second.
*         PITCH = non-dimensional pitch rate.
*         CHORD = chord-length of Joukowski airfoil.
*         ANGLE = radial of a given point on the circular cylinder.
*         UINF = freestream velocity, in feet per second.
*         CON = conversion factor, degrees to radians.
*         X,Y,U = coordinates and potential flow velocity on airfoil.
*         Z,W = complex coordinates and velocity.
*         UMIN = ratio of wall velocity to potential flow velocity.
*         TIME = cumulative time.
*         DELT = increment of time.
*         K,N = integer counters.
*         DSS = increment of distance on the airfoil surface.
*         DUDS = spatial partial derivative of velocity.
*         DUDT = partial derivative of velocity wrt time.
*         XOC = chord position.
*         BETA = local slope of airfoil surface.
*         RAS1,RAC1 = functions (of geometry) due to pitching motion.
*         RLAMDA,RK = Pohlhausen shape parameters.
*         FK,ZZ,DZDS,DEL2,F1K = functions of shape parameters.
*
      PROGRAM POHL6
      COMPLEX EI
      OPEN (15,FILE='FLOWIN')
      REWIND 15
      OPEN (16,FILE='FLOWOUT')
      REWIND 16
      EI=(0.,1.)
      RADIUS=1.131
      AMU=-.131
      READ (15,*) ALPHA,ADOT1,UINF
      ALPH1=ALPHA
      CON=3.1415927/180.
      ADOT2=ADOT1*CON
      THETA=180.
      TIME=0.0
      CALL DS(180.,RADIUS,CON,AMU,XLE,YLE)
      CALL DS(0.0,RADIUS,CON,AMU,XTE,YTE)
      XLE=ABS(XLE)
      CHORD=XLE+XTE
      PITCH=ADOT1*CON*0.5*CHORD/UINF
*
      K=100
      K1=K+1
```

```
      K2=(ALPHA+15Ø)*1ØØ+K
*
      WRITE(16,3Ø)UINF
      WRITE(16,4Ø)ALPHA
      WRITE(16,5Ø)ADOT1
      WRITE(16,52)
*
      ANGLE=ALPHA+THETA
      CALL U(ANGLE,RADIUS,CON,EI,UINF,AMU,ALPHA,UØ)
      CALL DS(ANGLE,RADIUS,CON,AMU,XØ,YØ)
      ANGLE=ANGLE-Ø.Ø1
      CALL U(ANGLE,RADIUS,CON,EI,UINF,AMU,ALPHA,U1)
      CALL DS(ANGLE,RADIUS,CON,AMU,X1,Y1)
      ANGLE=ANGLE-Ø.Ø1
      CALL U(ANGLE,RADIUS,CON,EI,UINF,AMU,ALPHA,U2)
      CALL DS(ANGLE,RADIUS,CON,AMU,X2,Y2)
      DS2=(SQRT((X2-X1)**2+(Y2-Y1)**2))/CHORD
      DS1=(SQRT((X1-XØ)**2+(Y1-YØ)**2))/CHORD
*
*     Stagnation point velocity gradient computed using a
*     forward difference method; all other velocity gradients
*     computed using central difference method.
*
      DUDS=(U2-UØ)/(DS1+DS2)
*
*     Second derivative of velocity computed using a
*     Taylor's series expansion.
*
      D2UDS2=(U2-2.*U1+UØ)/((DS1+DS2)/2.)**2
*
*     Enter initial boundary layer parameters.
*
      RLAMDA=7.Ø52
      RK=Ø.Ø77Ø
      FK=Ø.Ø
      DZDS=-Ø.Ø652*D2UDS2/(DUDS**2)
      ZZ=RK/DUDS
*
      N=5Ø
      ANGLE=ALPHA+THETA-Ø.Ø1
      XOC=(XØ+XLE)/CHORD
      WRITE(16,1)XOC,UØ,DUDS,D2UDS2,FK,RK,ZZ,DZDS
*
      ADOT=Ø.Ø
      DO 1Ø J=1,K
*
*     Function of this loop is to compute boundary layer
*     parameters at stagnation point, allowing the
*     boundary layer to steady-out before subjecting it
*     to a pitching motion.
*
      N=N+1
*
*     Compute pertinent boundary layer parameters.
*
      ZZ=DZDS*DS1+ZZ
      RK=ZZ*DUDS
      FK=.47-6.*RK
      DZDS=FK/U1
*
      DELT=CHORD*DS1/U1
      TIME=TIME+DELT
      CALL U(ANGLE,RADIUS,CON,EI,UINF,AMU,ALPHA,U2)
      DUDT=(U2-U1)/DELT
```

```
      ANGLE=ANGLE-Ø.Ø1
      ANGLE1=ANGLE-Ø.Ø1
      CALL U(ANGLE1,RADIUS,CON,EI,UINF,AMU,ALPHA,U2)
      CALL DS(ANGLE1,RADIUS,CON,AMU,X2,Y2)
      ANGLEØ=ANGLE+Ø.Ø1
      CALL U(ANGLEØ,RADIUS,CON,EI,UINF,AMU,ALPHA,UØ)
      CALL DS(ANGLEØ,RADIUS,CON,AMU,XØ,YØ)
      CALL U(ANGLE,RADIUS,CON,EI,UINF,AMU,ALPHA,U1)
      CALL DS(ANGLE,RADIUS,CON,AMU,X1,Y1)
      DS1=(SQRT((X1-XØ)**2+(Y1-YØ)**2))/CHORD
      DS2=(SQRT((X2-X1)**2+(Y2-Y1)**2))/CHORD
*
*     Compute the arc length and the velocity gradient.
*
      DSS=DS1+DS2
      DUDS=(U2-UØ)/DSS
      XOC=(X1+XLE)/CHORD
      IF(N.LT.5Ø) GO TO 1Ø
      N=Ø
      WRITE(16,1)XOC,U1,DUDS,DUDT,FK,RK,ZZ,DZDS
 1Ø   CONTINUE
*
      ADOT=ADOT1
      N=Ø
      RAS1=Ø.Ø
      RAC1=Ø.Ø
      DO 2Ø J=K1,K2
*
*     Function of this loop is to compute the behavior
*     of the boundary layer as it is subjected to a
*     pitching motion.
*
      N=N+1
*
*     Compute the pertinent boundary layer parameters.
*
      ZZ=DZDS*DS1+ZZ
      RK=ZZ*(DUDS*(1.+RAS1/U1)+DUDT/U1)
      CALL POHL(RK,RLAMDA)
      DEL2=37./315.-RLAMDA/945.-(RLAMDA**2)/9Ø72.
      FK=2.*DEL2*(2.-.3683*RLAMDA+.Ø1Ø4*RLAMDA**2+
     +  (RLAMDA**3)/4536.)
      F1K=(.3-RLAMDA/12Ø.)/DEL2
      DZDS=(FK+(4.+F1K)*ZZ*DUDT/U1+(4.+2.*F1K-2./DEL2)*ZZ
     +  *RAS1*DUDS/U1-8.*ZZ*RAC1/DEL2)/U1
*
*     Compute the time increment for a particle to
*     travel from point (i) to point (i+1).
*
      DELT=CHORD*DS1/U1
      TIME=TIME+DELT
      DALPHA=DELT*ADOT
      ANGLE=ANGLE+DALPHA
      ALPH1=ALPH1+DALPHA
      CALL U(ANGLE,RADIUS,CON,EI,UINF,AMU,ALPH1,U2C)
      CALL NIU(ANGLE,RADIUS,CON,AMU,ADOT2,X1,Y1,U2C,U2,RAS2,RAC2)
*
*     Compute the unsteady velocity gradient.
*
      DUDT=(U2-U1)/DELT
      ANGLE=ANGLE-Ø.Ø1
      ANGLE1=ANGLE-Ø.Ø1
      CALL U(ANGLE1,RADIUS,CON,EI,UINF,AMU,ALPH1,U2C)
      CALL DS(ANGLE1,RADIUS,CON,AMU,X2,Y2)
```

```
      CALL NIU(ANGLE1,RADIUS,CON,AMU,ADOT2,X2,Y2,U2C,U2,RAS2,RAC2)
      ANGLEØ=ANGLE+Ø.Ø1
      CALL U(ANGLEØ,RADIUS,CON,EI,UINF,AMU,ALPH1,UØC)
      CALL DS(ANGLEØ,RADIUS,CON,AMU,XØ,YØ)
      CALL NIU(ANGLEØ,RADIUS,CON,AMU,ADOT2,XØ,YØ,UØC,UØ,RASØ,RACØ)
      CALL U(ANGLE,RADIUS,CON,EI,UINF,AMU,ALPH1,U1C)
      CALL DS(ANGLE,RADIUS,CON,AMU,X1,Y1)
      CALL NIU(ANGLE,RADIUS,CON,AMU,ADOT2,X1,Y1,U1C,U1,RAS1,RAC1)
*
*     Compute arc length and velocity gradient.
*
      DS1=(SQRT((X1-XØ)**2+(Y1-YØ)**2))/CHORD
      DS2=(SQRT((X2-X1)**2+(Y2-Y1)**2))/CHORD
      DSS=DS1+DS2
      DUDS=(U2-UØ)/DSS
      UDUDS=U1*DUDS
      XOC=(X1+XLE)/CHORD
*
*     Stop the computation at the quarter-chord.
*
      IF(XOC.GE.Ø.25Ø) GO TO 25
      IF(N.LT.25Ø) GO TO 2Ø
      N=Ø
      WRITE(16,1)XOC,U1,DUDS,DUDT,FK,RK,ZZ,DZDS
 2Ø   CONTINUE
*
 25   WRITE(16,1)XOC,U1,DUDS,DUDT,FK,RK,ZZ,DZDS
      WRITE(16,45)ALPH1
      WRITE(16,55)PITCH
      WRITE(16,6Ø)RK
      WRITE(16,8Ø)
      WRITE(16,81)TIME
      UMIN=RAS1/U1
      WRITE(16,85)UMIN
  1   FORMAT(4X,F6.3,2(4X,F1Ø.3),4X,F7.3,4X,F7.4,4X,F8.4,2(4X,E9.3))
 3Ø   FORMAT(1H1,"BOUNDARY-LAYER PARAMETERS FOR ",F6.2,"FT/SEC"/)
 4Ø   FORMAT(" INITIAL ANGLE OF ATTACK: ",F6.3," DEGREES"/)
 45   FORMAT(/" FINAL ANGLE OF ATTACK: ",F6.3," DEGREES"/)
 5Ø   FORMAT(" PITCH RATE: ",F7.3," DEGREES/SEC"/)
 52   FORMAT(6X,"XOC",1ØX,"U",11X,"DUDS",9X,"DUDT",8X,"FK",
     + 9X,"RK",11X,"Z",11X,"DZDS"/)
 55   FORMAT(" PITCH PARAMETER: ",F7.5/)
 6Ø   FORMAT(" K AT THE QUARTER-CHORD: ",F8.4/)
 8Ø   FORMAT(" TIME TO REACH THE QUARTER-")
 81   FORMAT(" CHORD FROM THE STAGNATION POINT: ",F7.5," SEC"/)
 85   FORMAT(" UWALL/UE AT THE QUARTER-CHORD: ",E9.3/)
*
      STOP
 1ØØ  END
*
*
      SUBROUTINE U(ANGLE,RADIUS,CON,EI,UINF,AMU,ALPHA,UU)
      COMPLEX CMPLX,Z,EI,DZETA,W
*
*     Function of this subroutine is to to compute the local
*     value of velocity on a Joukowski airfoil using complex
*     potential flow theory.
*
      X=RADIUS*COS(ANGLE*CON)
      Y=RADIUS*SIN(ANGLE*CON)
      Z=CMPLX(X,Y)
      W=UINF*((1.,Ø.)-(RADIUS**2)/Z**2+
     + (2.*EI*RADIUS*SIN(ALPHA*CON))/Z)
      X=X+AMU
```

```
*
*       Z changed to represent values of coordinates used in
*       the transformation equation.
*
        Z=CMPLX(X,Y)
        DZETA=(Z**2-(RADIUS+AMU)**2)/Z**2
        UU=CABS(W)/CABS(DZETA)
        RETURN
        END
*
*
        SUBROUTINE DS(ANGLE,RADIUS,CON,AMU,X,Y)
        COMPLEX CMPLX,Z
*
*       Function of this subroutine is to compute the arc
*       length between two points on the Joukowski airfoil.
*
        X=RADIUS*COS(ANGLE*CON)+AMU
        Y=RADIUS*SIN(ANGLE*CON)
        Z=CMPLX(X,Y)
        Z=Z+((RADIUS+AMU)**2)/Z
        X=REAL(Z)
        Y=AIMAG(Z)
        RETURN
        END
*
*
        SUBROUTINE POHL(RK,RLAMDA)
*
*       Function of this subroutine is to compute the value
*       of the separation parameter, lamda, given a value
*       of K, as computed in the main program.
*
        RK1=-.160
        RK2=-.112
        RK3=0.00
        RK4=0.06
        RK5=0.076
        RK6=0.086
        RK7=0.0949
        IF(RK.LE.RK1) GO TO 10
        IF(RK.LE.RK2) GO TO 20
        IF(RK.LE.RK3) GO TO 30
        IF(RK.LE.RK4) GO TO 40
        IF(RK.LE.RK5) GO TO 50
        IF(RK.LE.RK6) GO TO 60
        IF(RK.GT.RK7) GO TO 70
*
        RLAMDA=.0149**2-(RK-0.08)**2
        RLAMDA=12.-100.*SQRT(RLAMDA)
        RETURN
*
  10    RLAMDA=(2./.012)*RK+14.0
        RETURN
*
  20    RLAMDA=(4./.044)*RK+2.18
        RETURN
*
  30    RLAMDA=(10./.14)*RK
        RETURN
*
  40    RLAMDA=83.33*RK
        RETURN
*
```

```
   50     RLAMDA=-1.9+115.*RK
          RETURN
*
   60     RLAMDA=-6.54+176.*RK
          RETURN
*
   70     RLAMDA=12.
          RETURN
          END
*
*
          SUBROUTINE NIU(ANGLEC,RADIUS,CON,AMU,ADOT2,XC,YC,UC,UNI,
     +    RASF,RACF)
*
*         Function of this subroutine is to compute the value of U in
*         the non-inertial reference frame, and the values of the
*         required functions of geometry.
*
          R=SQRT(XC**2+YC**2)
          BET1=ATAN(YC/(-XC))
          ANGLEM=ANGLEC+.1
          ANGLEP=ANGLEC-.1
          CALL DS(ANGLEM,RADIUS,CON,AMU,XM,YM)
          CALL DS(ANGLEP,RADIUS,CON,AMU,XP,YP)
          DY=ABS(YP-YM)
          DX=ABS(XP-XM)
          Q=1000.*DX
          IF(DY.GT.Q)THEN
          BETA=1.5707963
          ELSE
          BETA=BET1+ATAN(DY/DX)
          END IF
          RASF=R*ADOT2*SIN(BETA)
          RACF=R*ADOT2*COS(BETA)
          UNI=UC-RASF
          RETURN
          END
*
*
*
```

Vita

Major John S. Lawrence was born on 28 November 1950 in Marion, Ohio. He graduated from Pleasant Local High School in 1968 and was accepted into the Corps of Cadets at the United States Military Academy. Upon graduation from West Point in 1972, he received the degree of Bachelor of Science and a commission in the United States Army. He graduated from Rotary Wing Flight School in 1975, and has served in leadership positions in infantry, armor, and aviation units both stateside and overseas. In June 1982 he entered the School of Engineering, Air Force Institute of Technology. Major Lawrence and his wife, Kerry, currently reside in Xenia, Ohio, with their two children, Pete and Megan.

REPORT DOCUMENTATION PAGE

1a. REPORT SECURITY CLASSIFICATION: UNCLASSIFIED	1b. RESTRICTIVE MARKINGS
2a. SECURITY CLASSIFICATION AUTHORITY	3. DISTRIBUTION/AVAILABILITY OF REPORT: Approved for public release; distribution unlimited.
2b. DECLASSIFICATION/DOWNGRADING SCHEDULE	
4. PERFORMING ORGANIZATION REPORT NUMBER(S): AFIT/GAE/AA/83D-12	5. MONITORING ORGANIZATION REPORT NUMBER(S)
6a. NAME OF PERFORMING ORGANIZATION: School of Engineering; 6b. OFFICE SYMBOL (If applicable): AFIT/EN	7a. NAME OF MONITORING ORGANIZATION
6c. ADDRESS (City, State and ZIP Code): Air Force Institute of Technology, Wright-Patterson AFB, Ohio 45433	7b. ADDRESS (City, State and ZIP Code)
8a. NAME OF FUNDING/SPONSORING ORGANIZATION; 8b. OFFICE SYMBOL (If applicable)	9. PROCUREMENT INSTRUMENT IDENTIFICATION N
8c. ADDRESS (City, State and ZIP Code)	10. SOURCE OF FUNDING NOS.
11. TITLE (Include Security Classification): See Box 19	PROGRAM ELEMENT NO. / PROJECT NO. / TASK NO. / WORK UNIT NO.
12. PERSONAL AUTHOR(S): John S. Lawrence, B.S., Major, USA	
13a. TYPE OF REPORT: MS Thesis; 13b. TIME COVERED: FROM _____ TO _____	14. DATE OF REPORT (Yr., Mo., Day): 1983 December; 15. PAGE COUNT: 109
16. SUPPLEMENTARY NOTATION	Approved for public release: IAW AFR 190-17. LYNN E. WOLAVER, Dean for Research and Professional Development, Air Force Institute of Technology (AFIT). 3 JAN 1984

17. COSATI CODES		
FIELD	GROUP	SUB. GR.
20	04	

18. SUBJECT TERMS (Continue on reverse if necessary and identify by block number): Dynamic Stall, Pitching Airfoil, Boundary Layer, Unsteady Momentum-Integral Method, MRS Model, Mass Introduction

19. ABSTRACT (Continue on reverse if necessary and identify by block number)

Title: INVESTIGATION OF EFFECTS CONTRIBUTING TO DYNAMIC STALL USING A MOMENTUM-INTEGRAL METHOD

Thesis Chairman: Eric J. Jumper, Major, USAF

20. DISTRIBUTION/AVAILABILITY OF ABSTRACT: UNCLASSIFIED/UNLIMITED ☒ SAME AS RPT. ☐ DTIC USERS ☐	21. ABSTRACT SECURITY CLASSIFICATION: UNCLASSIFIED
22a. NAME OF RESPONSIBLE INDIVIDUAL: Eric J. Jumper, Major, USAF	22b. TELEPHONE NUMBER (Include Area Code): 513-255-3517; 22c. OFFICE SYMBOL: AFIT/ENY

Dynamic stall effects are analyzed in this investigation for cases of (1) an inertially static airfoil in a flow field rotating at constant rate (gust response), and (2) an airfoil pitching at constant rate in a steady flow field. The method used is a boundary layer solution of the momentum-integral equation by a modified von Karman-Pohlhausen technique.

Work accomplished by Docken in 1982 using this method to match Kramer's experimental results for gust response is reviewed, corrected, and continued. The validity of the closure equation and the assumptions key to its derivation are examined, concluding that the closure equation is justified. A better match of Kramer's airfoil sections results in dynamic stall predictions very close to experimental data. The effect of varying airfoil thickness and camber is investigated.

By consideration of the non-Newtonian motion of the boundary layer on the surface of a pitching airfoil, the momentum-integral method is extended to the second case. Using the Moore-Rott-Sears model for flow separation criteria, analytical results were computed and compared with experimental data. Reduction in adversity of the pressure gradient accounts for only a fraction of the total dynamic effect, and it is proposed that mass introduction into the boundary layer from the free-stream may be a strongly contributing factor. This phenomena is demonstrated to have a large effect, and an argument is presented for the proper amount of mass introduction.

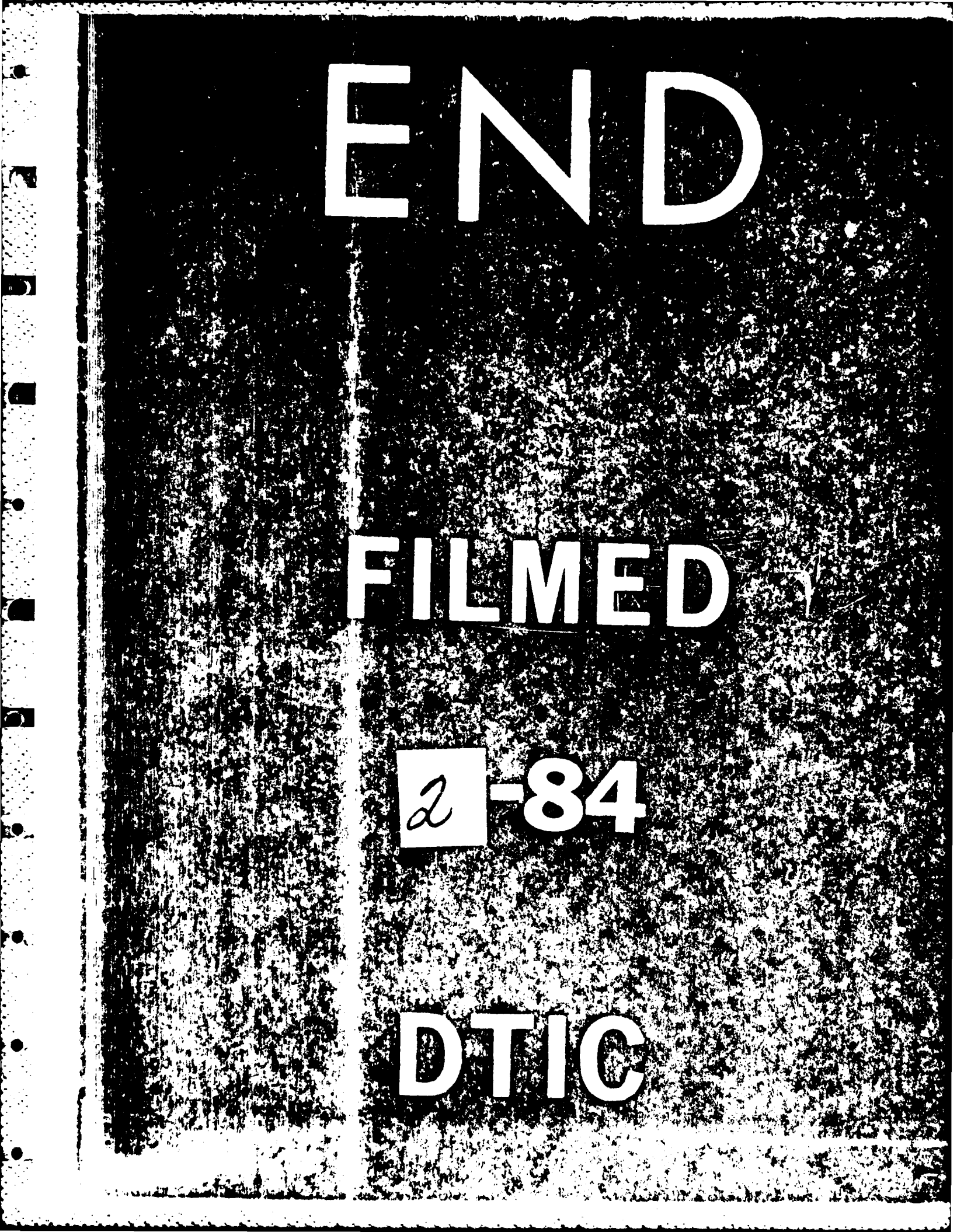
END
FILMED
2-84
DTIC